

# The Tolman Surface Brightness Test for the Reality of the Expansion. IV. A Measurement of the Tolman Signal and the Luminosity Evolution of Early-Type Galaxies

Lori M. Lubin<sup>1,2</sup>

*Department of Astronomy, California Institute of Technology,  
Mailstop 105-24, Pasadena, California 91125*

Allan Sandage

*Observatories of the Carnegie Institution of Washington,  
813 Santa Barbara Street, Pasadena, California 91101*

## ABSTRACT

We review a sample of the early literature in which the reality of the expansion is discussed. Hubble's reticence, even as late as 1953, to accept the expansion as real is explained as due to his use of equations for distances and absolute magnitudes of redshifted galaxies that do not conform to the modern Mattig equations of the standard model. The Tolman surface brightness test, once the only known test for the reality of the expansion, is contrasted with three other modern tests. These are (1) the time dilation in Type Ia supernovae light curves, (2) the temperature of the relic radiation as a function of redshift, and (3) the surface brightness normalization of the Planckian shape of the relic radiation.

We search for the Tolman surface brightness depression with redshift using the *Hubble Space Telescope* (HST) data from Paper III for 34 early-type galaxies from the three clusters Cl 1324+3011 ( $z = 0.76$ ), Cl 1604+4304 ( $z = 0.90$ ), and Cl 1604+4321 ( $z = 0.92$ ). Depressions of the surface brightness relative to the zero-redshift fiducial lines in the mean surface brightness, log linear radius diagrams of Paper I are found for all three clusters. Expressed as the exponent,  $n$ , in  $2.5 \log(1+z)^n$  mag, the value of  $n$  averaged over Petrosian radii of  $\eta = 1.7$  and  $\eta = 2.0$  for all three clusters is  $n = 2.59 \pm 0.17$  in the  $R$  band and  $3.37 \pm 0.13$  in the  $I$  band for a  $q_o = \frac{1}{2}$  model. The sensitivity of the result to the assumed value of  $q_o$  is shown to be less than 23% between  $q_o = 0$  and  $+1$ . The conclusion is that the exponent on  $(1+z)$  varies from 2.28 to 2.81 ( $\pm 0.17$ ) in the  $R$  band and 3.06 to 3.55 ( $\pm 0.13$ ) in the  $I$  band, depending on the value of  $q_o$ . For a true Tolman signal with  $n = 4$ , the luminosity evolution in the look-back time, expressed as the exponent in  $2.5 \log(1+z)^{4-n}$  mag, must then be

---

<sup>1</sup>Hubble Fellow

<sup>2</sup>Current address : Department of Physics and Astronomy, Johns Hopkins University, Baltimore, MD 21218

between 1.72 to 1.19 ( $\pm 0.17$ ) in the  $R$  band and 0.94 to 0.45 ( $\pm 0.13$ ) in the  $I$  band. We show that this is precisely the range expected from the evolutionary models of Bruzual & Charlot (1993, ApJ, 405, 538) and other measurements of the luminosity evolution of early-type galaxies. We conclude that the Tolman surface brightness test is consistent with the reality of the expansion to within the combined errors of the observed  $\langle SB \rangle$  depression and the theoretical correction for luminosity evolution.

We have also used the high-redshift HST data to test the “tired light” speculation for a non-expansion model for the redshift. The HST data rule out the “tired light” model at a significance level of better than  $10\sigma$ .

*Subject headings:* galaxies: clusters: general – cosmology: observations

## 1. Introduction

### 1.1. Early Commentaries on the Reality of the Expansion

With the announcement by Hubble (1929a) of a correlation between his estimates of distances to nearby galaxies and their redshifts, observational cosmology came of age, beginning its Long Journey into Night. The redshifts used by Hubble had been measured by Slipher, published by Eddington (1923), and added to by Humason (1929) in his crucial extension to higher values before Hubble’s announcement.

However, the announcement of an expanding universe was such an extraordinary claim that proof of its reality by some independent means seemed essential, even though an expanding universe had been predicted by Friedmann (1922) [cf. Tropp, Frenkel & Chernin 1993] as one of the solutions of fundamental Einstein equation of general relativity. Expanding solutions were also detailed later by Lemaitre (1927, 1931) and Robertson (1928), each of which, acknowledging Friedmann, made advances beyond Friedmann by their adumbrations concerning the available observations of galaxies and their relative distances.

It is not clear whether Hubble knew of the Friedmann (1922) prediction or of the theoretical, cum observational, papers of Lemaitre and Robertson in 1927 and 1928, although Robertson told one of us (AS) that he had discussed with Hubble the existence of an expanding solution to the Einstein equations before 1929 (e.g. Sandage 1995, footnote 16 to Chapter 5). None of these three principal theoreticians are mentioned in Hubble’s 1929 announcement.

Nevertheless, the decade of the 1920’s was not entirely free of observational attempts to test a related cosmological prediction. A year after the publication of Einstein’s field equations, de Sitter (1917a,b) had discovered one curious solution to them. Although his solution was that of a static metric (there are only three such solutions; Tolman 1929), it remarkably exhibited a redshift. The metric coefficient of the four-space time coordinate was a function of distance from the observer. Clocks that are further from the observer’s origin in the three-space manifold would appear to tick

more slowly than clocks at that origin. This effect would give an apparent redshift that would vary with distance. The formal feature of a redshift in the de Sitter metric was called “the de Sitter effect.” A curious additional feature was that any test particle put into the de Sitter manifold would exhibit a radial motion (Eddington 1923, §70; de Sitter 1933; Tolman 1934, §144–145)<sup>3</sup> even though the spatial metric was static.

The predicted existence of the de Sitter redshift effect with its static metric became well known in the decade of the 1920’s. Many attempts were made to find the effect using astronomical data (distances and velocities) for objects such as stars and globular clusters, thought then to comprise the wider universe before Hubble (1925, 1926, 1929b) proved the existence of external galaxies. Among the most accessible papers concerning the search for the de Sitter effect are those by Silberstein (1924), Stromberg (1925), Wirtz (1925), Lundmark (1925), and undoubtedly many others.

With regard to the de Sitter effect, it is a continuing curiosity as to what Hubble meant in the final sentence of his announcement in 1929 where he wrote:

The outstanding feature is the possibility that the velocity-distance relation may represent the de Sitter effect.... In this connection it may be emphasized that the linear relation found in the present discussion is a first approximation *representing a restricted range in distance* (emphasis added).

In other words, a larger range in distance may not show a linear relation, he surmised, where he apparently knew that the first order de Sitter effect is *quadratic* in distance rather than linear (e.g. Sandage 1995, eq. 5.10). Cautiously, Hubble left open the possibility that the data which he had discussed might define a redshift-distance relation that would actually vary as the square of the distance, which, in first approximation, would appear to be linear for short distances near the origin (i.e. the first term of a Taylor series). Hubble also undoubtedly knew of the earlier searches for the de Sitter effect by Lundmark (1925) and Silberstein (1924) where they attempted parabolic fits to their adopted data.

However, Hubble & Humason (1931) soon proved that the redshift-distance relation was, in fact, linear over the much larger range of redshifts than was available in 1929. For this and other reasons, de Sitter (1933) wrote: “We know now, because of the observed expansion, that the actual universe must correspond to one of the non-static models.... The static models are, so to say, only of academic interest.”

---

<sup>3</sup>An accessible derivation of the de Sitter static metric and its properties is given by Tolman (1934, §136 and §142–145). A more recent summary of the de Sitter metric with its redshift properties is given elsewhere (Sandage 1975, §2.2).

## 1.2. Later Attempts to Counter the Reality of the Expansion

Nevertheless, the concept of an expanding universe seemed so bizarre to many commentators that attempts began already in 1929 to find alternate ways to produce large redshifts other than from a true expansion. These attempts continue to this day.

The first alternate suggestion was made by Zwicky (1929) where he proposed that photons lose energy on their way to us from a distant source. As a consequence, they would show a redshift in their energy distribution, both in the continuum radiation and in the Fraunhofer lines used to measure the redshifts. To first order, the redshift effect would be linear with distance because the first term in a Taylor expansion of  $1 + z = e^{\frac{HD}{c}}$  is linear in  $D$ . Here,  $H$  is the Hubble constant and  $D$  is the distance. With this suggestion, Zwicky (1929) introduced the notion of “tired light.”

Even as late as mid-twentieth century, Zwicky (1957) maintained that the hypothesis was viable. However, neither Zwicky nor any other subsequent supporter of the proposition (e.g. La Violette 1986; Pecker & Vigier 1987) gave a convincing physical theory for the “tiredness.” As critics still point out, any scattering process with energy transfer from the photon beam to the scattering medium, as required for a redshift, must broaden (deflect) the beam. This effect would cause images of distant galaxies to be fuzzier than their local counterparts, which they are not.

## 1.3. Hubble’s Reticence

Perhaps the most interesting attack on the reality of the expansion was the reluctance of Hubble himself to believe that the redshifts represent a true expansion rather than “caused by an unknown law of nature.” Much has been written about Hubble’s reluctance, most of which is wrong. Some commentators even suggest philosophical or religious reasons related to a presumed abhorrence of a “creation” event that is implied in some interpretations of a real Friedmann expansion.

However, the fact is that Hubble’s reasons were those of a reductionist bench scientist. He relied (mistakenly, it turns out) solely on the interpretation of his observational data and their accuracy, coupled with a mistaken theory of how redshifts should vary with “distance.” His equation for “distance” has no justification within the modern Mattig (1958) equations. This story, and why Hubble’s conclusion would not have been reached using current data analyzed with the modern theoretical equations, is set out in detail elsewhere (Sandage 1998).

In outline, Hubble’s argument was as follows. By the mid 1930’s, Hubble (1934; 1936a,b) had completed his program of galaxy counts, the goal of which was to measure the curvature of space. He also completed the extension of the Hubble diagram of redshift versus apparent magnitude to the limit of the Mount Wilson 100-inch reflector (Hubble 1936; Humason 1936). The data for each of these programs had to be corrected for the effects of redshifts on the apparent magnitudes. If the expansion was real, Hubble assumed that the observed bolometric magnitudes (or equivalently, the observed magnitudes corrected for the selective part of the  $K$  term) must be made brighter

by two factors of  $2.5 \log(1+z)$ ; however, if the redshift was due to “an unknown law of nature” rather than the expansion, only one such factor was to be applied to the observed magnitudes.

Hubble believed that the Hubble diagram (log of the redshift versus apparent magnitude) must be strictly linear; in addition, the radius of curvature of space implied by his “corrected” magnitudes for his galaxy counts must not be “too small.” Consequently, he became convinced that only one factor of  $2.5 \log(1+z)$  should be applied. If so, the expansion would not be real. Hubble (1936b) wrote:

If the redshifts are not primarily due to velocity shifts ... [then] the velocity-distance relation is linear; the distribution of nebulae is uniform; there is no evidence of expansion, no trace of curvature, no restriction of the time scale.... The unexpected and truly remarkable features are introduced by the additional assumption that redshifts measure recession. The velocity-distance relation deviates from linearity by the exact amount of the postulated recession. The distribution departs from uniformity by the exact amount of the recession. The departures are compensated by curvature which is the exact equivalent of the recession. Unless the coincidences are evidence of an underlying necessary relation between the various factors, they detract materially from the plausibility of the interpretation. The small scale of the expanding model, both in space and time, is a novelty and as such will require rather decisive evidence for its acceptance.

That “rather decisive evidence” is now available from at least three modern experiments that are independent of the Tolman galaxy surface brightness test.

## 1.4. Other Recent Proofs that the Expansion is Real

### 1.4.1. *The Time Dilation Test*

The Tolman (1930) surface brightness  $(1+z)^4$  effect was the only known test for the reality of the expansion until Wilson (1939) suggested that the shape of the light curves of Type Ia supernovae provides a clock. This supposition was based on the uniform shape of the light curve discovered by Baade (1938) and recalled as history by Minkowski (1964). Wilson reasoned that such clocks at different redshifts would measure the special relativity time dilation if the light curve shapes of SNe Ia at high redshifts could be observed. The stretching of the light curves, increasing with redshift, has now been observed. The data give a spectacular confirmation of the time dilation effect (Goldhaber et al. 1997, 2001).

#### 1.4.2. *Temperature of the Relic Blackbody Radiation as a Function of Redshift*

Blackbody radiation in an expanding cavity remains Planckian in shape but with a decreasing temperature that scales as  $T(z) = T(0)(1+z)$  with redshift (Tolman 1934, eq. 177.7; Bahcall & Wolf 1968). The observations of the Boltzman temperature of interstellar molecules in the spectra of high-redshift galaxies has now apparently been measured in a difficult experiment with the Keck 10-m telescopes (Songaila et al. 1994). An important confirmation of these first results was made in observations by Ge et al. (1997) and Srianand, Petitjean & Ledoux (2000). Only upper limits had been achieved before (cf. Meyer et al. 1986) which, nevertheless, were highly important in pioneering this test.

#### 1.4.3. *Measurement of the Chemical Potential the Alpher-Herman Relic Black Body Radiation*

Although the *shape* of an initial blackbody spectrum remains Planckian in an expanding cavity, the vertical normalization (i.e. the photon number) remains Planckian only if that normalization is decreased with redshift by  $(1+z)^4$ . This fact is derived trivially from the Planck equation as expressed in terms of energy flux per wavelength per unit wavelength interval rather than frequency per unit frequency interval. (Of course, both representations are equivalent by minding the relation between wavelength interval and frequency interval, where  $d\nu = c\frac{d\lambda}{\lambda^2}$ .)

Hence, because the Planck equation defines a *surface brightness*, a test of the Tolman surface brightness effect is equivalent to measuring the deviation of the photon number per unit surface area in the sky by comparing the observations with the normalization given by the Planck equation itself. The deviation of the data from the Planck equation is called the “chemical potential.” Among other things, the deviation with wavelength could be due to Compton scattering in the early universe.

No deviation has been found in the observations to within one part in  $10^4$ . The perfect Planckian shape of the relic radiation was measured with COBE to within this limit of  $9 \times 10^{-5}$  (Mather et al. 1990; Fixsen et al. 1996). The conclusion to be drawn from this spectacular result is that this seemingly perfect normalization of the spectral energy distribution is a definitive proof of the Tolman surface brightness factor and, therefore, a definitive proof of the reality of the expansion. We shall adopt this assumption later in §4 where we combine our surface brightness signal with the theoretical  $(1+z)^4$  Tolman signal and interpret the difference to be due to luminosity evolution in the high-redshift look-back time.

### 1.5. **Plan of the Present Paper**

In the first three papers of this series (Sandage & Lubin 2001, hereafter Paper I; Lubin & Sandage 2001a and 2001b, hereafter Papers II and III), we provide the background and observational

data required to carry out the Tolman test. Most importantly, we measure the fiducial (zero-redshift) relations between the mean surface brightness, absolute magnitude, and linear radius for local early-type galaxies in Paper I. In Paper III, we present the observational data on our high-redshift comparison sample of 34 early-type galaxies in the three clusters used in this program, Cl 1324+3011 at  $z = 0.76$ , Cl 1604+4304 at  $z = 0.90$ , and Cl 1604+4321 at  $z = 0.92$  (Oke, Postman & Lubin 1998; Postman et al. 1998, 2001; Lubin et al. 1998, 2001). To compare accurately the local and high-redshift data, the parameters of each galaxy are measured at discrete values of the Petrosian (1976)  $\eta$  metric radius, which is defined as the difference in magnitude between the mean surface brightness averaged over the area interior to a particular radius and the surface brightness at that radius (see §2 of Paper I).

In the present paper, we use the results presented in Papers I–III to complete the Tolman test. In §2 we review the Mattig (1958) cosmological equations with which to calculate the absolute magnitudes and linear radii of galaxies from their apparent magnitudes and angular radii. Explicit equations for the special case of  $q_o = \frac{1}{2}$  are given. We use these equations to obtain the total magnitude  $M$ , linear radius  $R$ , and mean surface brightness  $\langle SB \rangle$  as functions of five Petrosian  $\eta$  radii of 1.0, 1.3, 1.5, 1.7, and 2.0 mag for the 34 high-redshift early-type galaxies. Tables 2–4 list these values for  $q_o = \frac{1}{2}$  and  $H_o = 50 \text{ km s}^{-1} \text{ Mpc}^{-1}$ . These values are derived from the observational data listed in Paper III. The Tolman test is made in §3 based on the data in §2 and the comparison with the surface brightness data at zero redshift from Paper I.

In §4 we set out the theoretical evolutionary corrections, first, using the simplest model of passive evolution by main sequence burn-down in the HR diagram as a function of time and, second, using the sophisticated star-formation models of Bruzual & Charlot (1993), following earlier papers by Guiderdoni & Rocca-Volmerange (1987, 1988) and Rocca-Volmerange & Guiderdoni (1988).

In §5 we show the sensitivity of the observed Tolman signal to the assumed value of  $q_o = \frac{1}{2}$  used in the data of Tables 2–4. Proof that the “tired light” assumption does not fit the data by a large factor is given in §6. In §7, we discuss the systematic uncertainties in the Tolman test made here and describe plans to strengthen the present test.

## 2. Calculation of Absolute Magnitudes and Linear Radii for the High-Redshift Galaxies

Comparison of the high-redshift data in Paper III with the data for local galaxies in Paper I requires knowledge of absolute magnitudes (corrected for  $K$  term) and linear radii.

We have two options to calculate these values. (1) If we were to assume that the standard model that leads to the Mattig (1958, 1959) equations (which assume that the expansion is real) did not exist, the natural assumption is that the distance,  $D_o$ , at the time that light is received is related to redshift by  $D_o = \frac{cz}{H_o}$ . This was Hubble’s assumption throughout his work, including the last summary paper in his Darwin lecture (Hubble 1953). (2) Alternately, we can adopt the details

of the standard model by choosing a value for the deceleration parameter,  $q_o$  (Hoyle & Sandage 1956). We then use the Mattig (1958) equations to calculate the distance moduli,  $m - M$ , and the linear radii,  $R$ , from the observed angular radii.<sup>4</sup>

Because these equations already contain the Tolman  $(1 + z)^4$  factor, the test for the Tolman effect becomes one of consistency between the surface brightness observations and the predictions of the standard model. The argument of why this does not lead to a hermeneutical circularity was given in §5 of Paper I. We adopt option (2) in calculating the distance moduli and the linear radii of the program clusters. We treat only the  $q_o = \frac{1}{2}$  case of the standard model in this section. The cases for  $q_o = 0$  and  $+1$  are treated in §5 using the correction recipes in Table 8.

### 2.1. The Equations for $q_o = \frac{1}{2}$

For the  $q_o = \frac{1}{2}$  case with  $H_o = 50 \text{ km s}^{-1} \text{ Mpc}^{-1}$ , the Mattig equations reduce to

$$m - M = 5 \log [2(1 + z - \sqrt{1 + z})] + 43.89, \quad (2)$$

and

$$D_1 = \frac{2c}{H_o(1 + z)} \left[ 1 - \frac{1}{\sqrt{1 + z}} \right], \quad (3)$$

where  $D_1$  is the distance (in parsecs) when light left the galaxy at the observed redshift  $z$ . The linear radius  $R$ , in parsecs, of a galaxy with angular radius  $\theta$ , in radians, is

$$R(\text{pc}) = \frac{2c (\sqrt{1 + z} - 1)}{H_o(1 + z)^{\frac{3}{2}}} \theta(\text{radians}), \quad (4)$$

using the distance  $D_1$  from equation (3).

Changing the angular radius in radians to arcseconds, equation (4) can be conveniently written as

---

<sup>4</sup>To avoid confusion with our use of  $R$  in this paper to mean the linear radius of a galaxy rather than its use as the time-dependent scale factor in the metric, we have used  $D$  here as the distance parameter by replacing  $Rr$  by  $D$ , where, in the standard notation,  $R$  is the scale factor that varies with time and  $r$  is the dimensionless co-moving radial coordinate in the metric. Hence, in our notation here,  $D_o$  is the distance at the time light is received from a galaxy at redshift  $z$ . This is given by Mattig (1958; see also Sandage 1988, eq. 30) as

$$D_o = \frac{c}{H_o q_o^2 (1 + z)} [z q_o + (q_o - 1) \{-1 + \sqrt{2 q_o z + 1}\}] \quad (1)$$

$$\log R(\text{pc}) = \log \theta'' + \log A, \quad (5)$$

where

$$A = 5.818 \times 10^4 \left[ \frac{\sqrt{1+z}-1}{(1+z)^{\frac{3}{2}}} \right], \quad (6)$$

for  $q_o = \frac{1}{2}$  and  $H_o = 50$ .

Equations 2–4 are derived in Sandage (1961a,b; 1988; 1995), where the standard model is summarized from the point of view of practical cosmology.

Table 1 shows the  $m - M$  and  $A$  values for the three program clusters for the  $q_o = \frac{1}{2}$  case using equations (2), (5), and (6). The  $K$  terms are those derived in Paper III (see Table 4).

## 2.2. The $M$ , $R$ , and $\langle SB \rangle$ Data for the Three Program Clusters for the $q_o = \frac{1}{2}$ Case

The results for absolute magnitude  $M$ , linear radius  $R$ , and mean surface brightness  $\langle SB \rangle$  are listed in Tables 2–4 where the  $\langle SB \rangle$  values are those in Paper III, corrected for the effects of redshift by the  $K$  terms from Table 1. The format of Tables 2–4 is the same as for Tables 5–7 in Paper III. Data for the five  $\eta$  values of 1.0, 1.3, 1.5, 1.7, and 2.0 are listed. For each  $\eta$ , the  $K$ -corrected absolute magnitude is calculated using the  $m - M$  value from Table 1 and the apparent magnitudes from Paper III. The  $K$ -corrected mean surface brightnesses from Paper III are given next. The logs of the linear radii (in parsecs) are obtained by adding the log of the angular radii from Tables 5–7 of Paper III to the  $A$  values from Table 1, calculated using equations (5) and (6).

## 3. The Tolman Test Using the HST Data for Early-Type Galaxies from the Three Program Clusters for $q_o = \frac{1}{2}$

The data that are necessary to make the Tolman test are given in Tables 2–4. The search for a Tolman signal, as modified by luminosity evolution, is made by comparing these high-redshift data with the calibrations at zero redshift in Paper I. The comparisons for the  $R$  photometric band of cluster Cl 1604+4321 ( $z = 0.9243$ ) can be made directly because the Postman & Lauer (1995) calibrations in Paper I are already in the standard Cape/Cousins  $R$  photometric band.

Comparisons in the  $I$  band for clusters Cl 1324+3011 ( $z = 0.7565$ ) and Cl 1604+4304 ( $z = 0.8967$ ) are made by converting the calibrations in Paper I to the  $I$  photometric band by applying the adopted color of  $\langle R - I \rangle = 0.62$ . This mean  $(R - I)$  color for early-type galaxies at zero redshift was derived by (1) using  $\langle B - R \rangle = 1.52$  from the photometry of Postman & Lauer (1995), as

corrected for  $K$  term and Galactic absorption in Paper I, and (2) using the two-color  $(B - R)$ ,  $(R - I)$  diagram from the data of Poulain & Nieto (1994) to give  $\langle R - I \rangle = 0.62$  at  $\langle B - R \rangle = 1.52$ . A color of  $\langle R - I \rangle = 0.62$  corresponds to a mean stellar spectral type of about K5 (see Figure 10 of Sandage 1997).

### 3.1. The Tolman Signal in the $\log R$ , $\langle SB \rangle$ Correlation Diagram

We approach the problem first by considering the data in the parameter space which contains the smallest evolutionary signal and, therefore, is expected to have the strongest Tolman signal (if it exists). Beyond a doubt, luminosity evolution occurs in a stellar population with no new star formation after the first initial star burst. The main sequence termination point in the Hertzsprung–Russell (HR) diagram burns down to fainter luminosities as the population ages, making the total luminosity of the aggregate fainter with time. Calculation of the burn-down rate, coupled with the luminosity function that determines relative numbers of stars that partake in the evolution, gives a first estimate of the change of total luminosity with time. This is how we make a first estimate of the effect in §4.

Luminosity evolution affects both the observed surface brightness and the absolute magnitude. However, we expect that it does not affect the radius as a function of time. The consequence is that the correlation of surface brightness versus absolute magnitude has a double dose of evolution because both coordinates are affected, whereas the correlation of surface brightness and linear radius contains only a single dose, on the assumption that the radius does not change. On this basis, the most powerful of the three correlation diagrams from Paper I is the  $\langle SB \rangle$ ,  $\log R$  diagram. In this section we examine this correlation, searching for a Tolman signal in each of the three high-redshift clusters.

#### 3.1.1. The data in $R$ for Cl 1604+4321 ( $z = 0.9243$ )

Figure 1 shows the  $\langle SB \rangle$ ,  $\log R$  correlation diagram for Cl 1604+4321 in the  $R$  photometric band as corrected for  $K$  dimming using Table 1. Large dots are those galaxies in Table 2 that have directly measured redshifts. Small dots are assumed cluster members on the basis of their photometric redshifts (for details, see Paper III).

The lines in each panel are the correlations for zero redshift from Tables 2 and 3 of Paper I based on the photometry by Postman & Lauer (1995) and extended to radii smaller than  $\log R = 4.3$  using the data of Sandage & Perelmuter (1991). Note that Table 3 in Paper I lists the magnitude difference between the best-fit relations of the Sandage & Perelmuter (1991) and the Postman & Lauer (1995) data; therefore, the best-fit lines given in Table 2 of Paper I need to be made *fainter* by the absolute value of the corrections listed in Table 3 of Paper I. The resulting local lines carry an error in the  $\langle SB \rangle$  vertical position that varies between 0.04 mag and 0.50 mag

depending on  $\log R$  (see Table 3 of Paper I).

*The effect for which we are searching is clearly seen in Figure 1.* It is the depressed surface brightness at a given radius compared with the surface brightness of early-type galaxies at zero redshift. We interpret this depression to be the Tolman signal as diluted by luminosity evolution.

The amount of the depression for each galaxy was calculated relative to the zero-redshift line at a given radius. This is done by using the equations for the zero-redshift lines from Tables 2 and 3 of Paper I and subtracting the observed  $\langle SB \rangle$  values for each galaxy from these fiducial lines read at the same  $\log R$  value. The subsequent errors on this difference in mean surface brightness include both the measurement error in the  $\langle SB \rangle$  of the galaxy and the uncertainties in the local line (see Tables 2–3 of Paper I). The result for Cl 1604+4321 is listed in Table 5 as the mean depressions for the five Petrosian  $\eta$  radii of 1.0, 1.3, 1.5, 1.7, and 2.0 using all of the galaxies in Table 2.

Column 2 of Table 5 shows the depression in magnitudes from the local line which was calculated from a weighted average of the program galaxies in Cl 1604+4321. Column 3 of Table 5 gives the exponent,  $n$ , in  $2.5 \log(1+z)^n$  for the observed mean  $\Delta\langle SB \rangle$  depression, which are listed as magnitudes in column 2. With  $z = 0.9243$ , it follows that  $n = 1.407 \times \Delta\langle SB \rangle$  for Cl 1604+4321.

Column 4 of Table 5 shows the correction for luminosity evolution, in magnitudes, that is required in order to make the Tolman signal of  $2.5 \log(1+0.9243)^4 = 2.84$  mag, based on the argument in §1.4.3 that the true exponent must be 4 because of the black body normalization of the relic radiation. Therefore, column 4 is the difference between 2.84 mag and the listings in column 2. Column 5 shows the exponent,  $4 - n$ , for the luminosity evolution, expressed as  $\Delta M_{evol} = 2.5 \log(1+z)^{4-n}$  mag that is required to make the true Tolman signal  $(1+z)^4$ . Finally, column 6 shows the number of galaxies in Cl 1604+4321 that are used in the averages.

Table 5 shows that the apparent Tolman signal in columns 2 and 3 dominates over the evolutionary requirements for luminosity evolution in columns 4 and 5. The exponent  $n$  varies from  $3.43 \pm 0.23$  to  $2.48 \pm 0.25$  for  $\eta$  radii from  $\eta = 1.0$  to 2.0 for Cl 1604+4321.

### 3.1.2. *The Data in I for the Two Clusters Cl 1324+3011 ( $z = 0.7565$ ) and Cl 1604+4304 ( $z = 0.8967$ )*

Figure 2 shows the combined data in the  $I$  band for the two clusters observed with HST in the  $F814W$  filter, reduced to the standard  $I$  system and corrected for  $K$  dimming by the values listed in Table 1. The  $M$  and  $\log R$  values listed in Tables 3 and 4 for these clusters are calculated from the Mattig (1958) equations using the  $m - M$  and  $\log A$  values listed in Table 1 and the observed data in Tables 5 and 6 of Paper III. Filled circles indicate the galaxies in Cl 1324+3011, while open circles indicate the galaxies in the higher-redshift cluster Cl 1604+4304. Again, the different symbol sizes separate the galaxies with measured redshifts from the assumed cluster members based on photometric redshifts (see Paper III).

The differences between the observed  $\langle SB \rangle$  magnitudes and the zero-redshift calibration values at a given radius, given as a weighted average over the galaxies in each cluster, are listed in Tables 6–7 in the same format as for Table 5. Column 2 shows the mean surface brightness depression from the zero-redshift fiducial line, expressed in magnitudes.

Column 3 shows the exponent on  $2.5 \log(1+z)$  to produce the listed mean values of these surface brightness depressions. Clearly,  $n = 1.635 \times \Delta\langle SB \rangle$  for Cl 1324+3011 ( $z = 0.7565$ ) and  $n = 1.439 \times \Delta\langle SB \rangle$  for Cl 1604+4304 ( $z = 0.8967$ ). The exponent  $n$  varies from  $4.15 \pm 0.25$  to  $3.25 \pm 0.25$  for Cl 1324+3011 and from  $4.20 \pm 0.26$  to  $3.29 \pm 0.30$  for Cl 1604+4304 for  $\eta$  radii from 1.0 to 2.0.

### 3.1.3. The Mean Tolman Signal From the Three Clusters

Tables 5–7 show the values of the mean depression in  $\langle SB \rangle$  and, therefore, the exponent  $n$  are a strong function of Petrosian radii  $\eta$ , being measured larger at smaller  $\eta$  values. This trend is a direct result of the finite angular resolution of the WFPC2 point-spread-function described in Paper II (Lubin & Sandage 2001a). Specifically, for smaller values of  $\eta$  we are not accurately measuring the true  $\eta(r)$  curve (see §2 of Paper II). As a result, we *underestimate* the mean surface brightness  $\langle SB(r) \rangle$  and, therefore, *overestimate* the signal, i.e. the depression from the zero-redshift relation. We have shown in Paper II that, even for the smallest galaxies with half-light radii of  $0''.25$ , the true  $\eta(r)$  curve is reached only for  $\eta \gtrsim 1.8$ . At these  $\eta$  values, the error in the measured mean surface brightness is less than 0.07 mag.

Therefore, in order to calculate our final numbers, we disregard the data at  $\eta$  values of less than 1.7 as undoubtedly unreliable at the  $> 0.1$  mag level. Consequently, we calculate the mean value of the exponent  $n$  averaged over the two  $\eta$  values of 1.7 and 2.0 only. We obtain a final value of the exponent  $n$  in the  $R$  band by using the data from Cl 1604+4321. For the  $I$  band, we note that the resulting values of the exponent  $n$  (as a function of  $\eta$ ) are the same within the errors for the two clusters observed in the  $I$  band, Cl 1324+3011 and Cl 1604+4304 (see Column 3 of Tables 5–7). Therefore, we have combined the data for both clusters for the final measurement in the  $I$  band.

As discussed above, we calculate the values for the depression  $\Delta\langle SB \rangle$  (as represented by the exponent  $n$ ) for the  $R$  and  $I$  bands from a weighted average of the data from  $\eta = 1.7$  and 2.0. The results for  $q_o = \frac{1}{2}$  are

$$\begin{aligned} \Delta\langle SB \rangle &= 2.5 \log(1+z)^{2.59 \pm 0.17} \text{ mag } (R \text{ Band}) \\ &2.5 \log(1+z)^{3.37 \pm 0.13} \text{ mag } (I \text{ Band}) \end{aligned} \tag{7}$$

for the apparent Tolman signal as compromised by luminosity evolution. The required luminosity

evolution would then be

$$\begin{aligned}
 M_{evol} &= 2.5 \log (1+z)^{1.41 \pm 0.17} \text{ mag (R Band)} \\
 &2.5 \log (1+z)^{0.63 \pm 0.13} \text{ mag (I Band)}
 \end{aligned}
 \tag{8}$$

We adopt equations (7) and (8) as our final values from the current experiment.

We must now test whether equation (8) is reasonable within the independent discipline of luminosity evolution of the stellar content using the precepts of population synthesis. In §4 we use the 1996 version of the Bruzual & Charlot (1993) models to test for compatibility between equation (8) and the stellar-population synthesis models. There is, of course, now a vast literature on population synthesis models. We have only used the Bruzual & Charlot (1993) models here. It will eventually be important to test for compatibility using different codes, such as earlier papers by Guiderdoni & Rocca-Volmerange (1987, 1988), Rocca-Volmerange & Guiderdoni (1988), and Worthey (1994).

### 3.2. The Doubly Diluted Tolman Signal in the $\langle SB \rangle$ , $M$ Correlation Diagram

In the last section we chose to analyze the data in the  $\langle SB \rangle$ , log R plane rather than in the  $\langle SB \rangle$ ,  $M$  plane as was done in Sandage & Perelmuter (1991). As explained in §3.1, the present method is preferred because it minimizes the effect of luminosity evolution, which, from the result in the last section, must be present at the level of  $2.5 \log (1+z)^{1.41 \pm 0.17}$  mag in the  $R$  band and  $2.5 \log (1+z)^{0.63 \pm 0.13}$  in the  $I$  band if the radius does not evolve over the look-back time and if the expansion is real. Nevertheless, it is of interest to examine the data in the  $\langle SB \rangle$ ,  $M$  correlation diagram that is doubly degenerate to the effects of luminosity evolution.

Figure 3 shows the data for Cl 1604+4321 in the  $R$  photometric band with the same symbols as in Figure 1. The data for the individual galaxies are from Table 2 and, therefore, refer to  $H_o = 50$  and  $q_o = \frac{1}{2}$  in calculating  $M$  from the redshift. The ordinate of  $\langle SB \rangle$ , as before, is independent of both  $H_o$  and  $q_o$  because it is given directly as observed, except that it has been corrected for  $K(R)$  dimming via Table 1.

We also plot in Figure 3 the envelope lines for the zero-redshift calibration. These relations have been calculated from the equations of  $\langle SB \rangle$  versus log R given in Table 2 of Paper I, as modified by the non-linearity corrections, given in Table 3 of Paper I, at radii smaller than log R = 4.3. We use equation (11) of Paper I, which gives  $\langle SB \rangle = M + 5 \log R(\text{pc}) + 22.815$ , to calculate the absolute magnitude  $M$  from the  $\langle SB \rangle$ , log R local relations. The resulting envelope lines, which are plotted in Figure 3, are the same to within the errors as the linear least-squares fits to the Postman & Lauer (1995) local data given in Table 4 of Paper I *over the overlapping linear range*.

Figure 4 shows the  $I$  band data for Cl 1324+3011 and Cl 1604+4304 as taken from Tables 3 and 4. The envelope lines plotted in this figure are the same as in Figure 3; however, they have been converted to the  $I$  band by  $\langle R - I \rangle = 0.62$  (see above).

Two features of Figures 3 and 4 are noted. (1) The scatter is larger than in the  $\langle SB \rangle$ , log R plane (Figures 1–2). (2) Although the mean  $\langle SB \rangle$  in both diagrams is depressed relative to the zero-redshift calibration lines, the amount is less in the  $\langle SB \rangle$ ,  $M$  plane than in the  $\langle SB \rangle$ , log R plane. The first effect on the larger scatter in Figures 3–4 is due to the larger scatter in the  $\langle SB \rangle$ ,  $M$  plane even for zero redshift (see Figure 3 of Paper I). The obvious reason is that errors in  $M$  and/or  $\langle SB \rangle$  move points *perpendicular* to the slope of the correlation line. By contrast, the error vectors in the  $\langle SB \rangle$ , log R plane in Figures 1 and 2 are nearly parallel to the correlation lines.

The second effect is due to the double degeneracy to luminosity evolution in the  $\langle SB \rangle$ ,  $M$  plane. As said before, luminosity evolution affects both coordinates. Relative to the zero-redshift line, an increase in the luminosity at high redshift due to luminosity evolution moves a point brighter in  $M$  and also brighter in  $\langle SB \rangle$  relative to that line. Therefore, in an observed  $\langle SB \rangle$ ,  $M$  diagram that contains luminosity evolution, the depression from the zero-redshift line is diluted twice, once in  $\langle SB \rangle$  and once in  $M$ .

Because Figures 1–2 are more powerful than Figures 3–4 for this reason of double degeneracy, we have made the calculations of the signal, as represented by  $n$ , and the luminosity evolution, as represented by  $4 - n$ , only from the  $\langle SB \rangle$ , log R data in Figures 1–2. Of course, the final answers from the analysis in either representation must be the same because the  $\langle SB \rangle$  versus log R and the  $\langle SB \rangle$  versus  $M$  diagrams are simply different representations of the same data, connected by equation (11) of Paper I.

### 3.3. The Tautological Absolute Magnitude Signal in the log R, $M$ Plane

Use of the Mattig (1958) equations for linear radius and absolute magnitude guarantees that the combination of  $\langle SB \rangle$ ,  $M$ , and the linear radius, R, are consistent with the variation of  $\langle SB \rangle$  with redshift as  $2.5 \log (1 + z)^4$  mag. Because the log R and  $M$  values in Tables 2–4 are calculated using the Mattig (1958) equations, the deviations of the “observed”  $M$ , calculated with the Mattig equation, must be precisely  $2.5 \log (1 + z)^{4-n}$ . Hence, the observed deviations from the zero-redshift lines prove nothing except to show how much the absolute magnitude,  $M$ , must change in the look-back time to conform with the  $\log (1 + z)^n + \log (1 + z)^{4-n} = \log (1 + z)^4$  relation.

In Figures 5 and 6, we plot the relation between log R and  $M$  for the  $R$  band and  $I$  band, respectively. The envelope lines are calculated from the zero-redshift relations using the linear equations from Table 2, the non-linear corrections for small R from Table 3, and equation (11) given in Paper I. These figures do nothing more than demonstrate that  $M$  *must* become brighter with increasing redshift (due to evolution) in order to make the true depression of  $\langle SB \rangle$  in Figures 1 and 2, corrected for evolution, equal to  $(1 + z)^4$  if the standard model is correct. From equation

(8), we see that the requirements for a precise agreement with the Tolman prediction is that the mean magnitude deviation at constant  $\log R$  must be  $\langle \Delta M \rangle = 0.39 \pm 0.08$  mag in the  $I$  band for Cl 1324+3011 ( $z = 0.7565$ ),  $\langle \Delta M \rangle = 0.44 \pm 0.09$  mag in the  $I$  band for Cl 1604+4304 ( $z = 0.8967$ ), and  $\langle \Delta M \rangle = 1.00 \pm 0.12$  mag in the  $R$  band Cl 1604+4321 ( $z = 0.9243$ ) if the Tolman signal, freed from luminosity evolution, would be precisely  $(1+z)^4$ . Calculating the average difference at constant  $\log R$  between the high-redshift data and the zero-redshift relations plotted in Figures 5 and 6, we measure precisely, by definition, these values. The predictions for luminosity evolution from spectral synthesis models with varying star formation histories are made in the next section to compare with these predictions from the Tolman test.

#### 4. Theoretical Luminosity Evolution Estimated Using Two Different Methods

##### 4.1. Elementary Estimate of the Correction for Passive Luminosity Evolution Due To Main Sequence Burn Down

An early order-of-magnitude estimate of the expected change of the luminosities of early-type galaxies in the look-back time was based on the change of the turnoff luminosity in the HR diagram for an old, coeval population where no new stars are formed after the initial starburst. The method is interesting because of its simplicity. It led early on to the result that the passive luminosity evolution correction was close to  $\Delta M_{bol} \sim \Delta M_V = 2.5 \log(1+z)$ . This result is given by the simplistic calculation of direct main sequence burn-down, including corrections for the main sequence luminosity function (Sandage 1961b, 1988). In addition, the elaborate population synthesis models by Tinsley (1968, 1972a,b, 1976, 1977, 1980 and references therein) gave nearly the same result.

We show in the next section that nearly the same result is also given by fitting the observed spectral energy distribution and the size of the 4000Å break with the star formation models of Bruzual & Charlot (1993). The look-back times vary, of course, with the assumed value of  $q_o$ . The calculated ages for galaxies with the observed redshifts of the three clusters must agree with the ages from the Bruzual & Charlot models, at least approximately, if our story is to have coherence. Anticipating the next section, we set out here the “cosmological ages” based on the redshift, the look-back time, and the assumed values of the Hubble constant  $H_o$  and  $q_o$ . The general case of the calculation of the look-back time for all values of  $q_o$  is solved elsewhere (Sandage 1961b). The special cases of  $q_o = 0$  and  $q_o = \frac{1}{2}$  are, of course, trivial. The ages,  $T$ , at a given redshift are given by

$$T = \frac{2H_o^{-1}}{3(1+z)^{\frac{3}{2}}}, \tag{9}$$

for  $q_o = \frac{1}{2}$  and

$$T = \frac{H_o^{-1}}{(1+z)}, \quad (10)$$

for  $q_o = 0$ .

The case for  $q_o = 1$  is more complicated and can be found from the tables in Sandage (1961b).

Equation (9) gives ages of 4.82 Gyr, 4.30 Gyr, and 4.21 Gyr at the time light left the three clusters with redshifts of 0.7565, 0.8967, and 0.9243, respectively, for  $q_o = \frac{1}{2}$  and  $H_o = 58 \text{ km s}^{-1} \text{ Mpc}^{-1}$ . For these calculations, we must use the real value of  $H_o$  (Sandage & Tammann 1997; Theureau et al. 1997; Saha et al. 1999; Sandage 1999; Parodi et al. 2000) rather than an arbitrary value as in previous sections because we need real ages in this section.

Equation (10) gives the ages at the time light left of 9.60 Gyr, 8.89 Gyr, and 8.76 Gyr, respectively, for the same clusters using  $q_o = 0$ . The extreme case of  $q_o = +1$ , where the age of the universe is only  $0.571 \times H_o^{-1} = 9.63 \text{ Gyr}$  for  $H_o = 58$ , gives ages when light left the three clusters of 3.77 Gyr, 3.32 Gyr, and 3.26 Gyr, respectively, using Table 3 of Sandage (1961b).

It is also interesting to calculate the absolute magnitudes of the main sequence termination ( $TO$ ) for these ages. The modern oxygen enhanced evolutionary models by Bergbush & Vandenberg (1992) for  $[\text{Fe}/\text{H}] = 0$  give bolometric magnitudes of

$$M(bol, TO) = 2.564 \log T(\text{yr}) - 21.644, \quad (11)$$

as interpolated from their tables (Sandage 1993). Hence, the main sequence absolute bolometric magnitudes for the  $q_o = \frac{1}{2}$  look-back times for the three clusters are 3.18, 3.06 and 3.03 mag, respectively. The brightest turn off magnitudes are, of course, for the  $q_o = +1$  models because the ages when light left are the smallest. These bolometric turnoff magnitudes for the  $q_o = +1$  case are 2.91, 2.79, and 2.73 mag, respectively.

#### 4.2. The Expected Evolution From the Bruzual & Charlot (1993) models

To calculate the expected amount of luminosity brightening with look-back time, we have chosen to use the stellar population synthesis code of Bruzual & Charlot (1993) because, as part of the original photometric and spectral analyses of these clusters, Postman, Lubin & Oke (1998, 2001; hereafter PLO98 and PLO01) use the 1996 stellar evolution models of Bruzual & Charlot (hereafter BC96) to study the star-formation histories and ages of the cluster galaxies. The authors find that the Bruzual & Charlot models are ideal because they can be used to generate absolute energy distributions over a broad wavelength range, with a spectral resolution which is comparable to the observed Keck spectra (see Oke, Postman & Lubin 1998; PLO98; PLO01).

The free parameters in the BC96 models include the mass function, the metal abundance, and

the star-formation rate. Following PLO98 and PLO01, we have chosen models with a Salpeter mass function (Salpeter 1955) and a maximum stellar mass of  $125 M_{\odot}$ . Comparisons with models constructed with a Scalo luminosity function (Scalo 1986) show no significant difference at the level of accuracy that can be achieved with low-resolution Keck spectra (PLO98). Based on the metal-line equivalent widths and balmer jump strengths, PLO01 determine that models with assumed metallicities between  $Z = 0.004$  (0.2 solar) and  $Z = 0.020$  (solar) provide reasonable fits to the data. Because the metallicities of the cluster galaxies are not strongly constrained, we assume a solar abundance for our calculations.

The most significant constraint on the BC96 models is the choice of the star formation history. The simplest model assumes that there is a large, initial burst of star formation after which the galaxy fades in accordance with passive stellar evolution models. These model are called “ssp” models by Bruzual & Charlot. The next simplest models are those where star formation begins at  $t = 0.0$  and decreases exponentially with a fixed time constant. PLO98 and PLO01 refer to these models as tau ( $\tau$ ) models and have considered time constants ranging from 0.2 to 20 Gyr. Any of these models can be used to generate the expected broad-band ( $BVRI$ ) AB magnitudes once the galaxy redshift is specified (see e.g. Figure 7 of Paper III).

In order to characterize the observed spectral energy distribution (SED) of each galaxy, PLO01 have used the slope, referred to as  $b$ , of a linear least-squares fit to the measured AB magnitudes as a function of  $\log \nu$  (see §2.1 of PLO01). The slope  $b$  provides a more robust indicator of the overall broad-band SED than any individual color measure, although  $b$  is strongly correlated with the usual broad-band colors [e.g.  $(V - R) \approx \frac{b}{13}$ ]. The early-type galaxies used in the present experiment are the reddest galaxies in the clusters and, therefore, have the largest values of slope  $b$  with  $b \gtrsim 10$  (see Tables 2–4 of PLO01). The best-fit BC96 models to these galaxies are either the ssp model (which is essentially equivalent to a  $\tau = 0.2$  Gyr model) or a tau model with  $\tau \leq 1.0$  Gyr (see Figure 6 of PLO01). Therefore, we have chosen these models to measure the range in luminosity evolution that we expect between  $z = 0$  and the cluster redshifts of  $z = \{0.7565, 0.8967, 0.9243\}$ , respectively.

For these calculations, we use the ages for each cluster derived in §4.1 for different values of  $q_o$  and assume that the epoch of star formation occurred at  $z_{form} \gtrsim 2.5$ . This high formation epoch is consistent with other observations of cluster early-type galaxies (e.g. Aragón-Salamanca et al. 1993; Stanford, Eisenhardt & Dickinson 1995, 1998; Oke, Gunn & Hoessel 1996; Ellis et al. 1997; van Dokkum et al. 1998; de Propis et al. 1999).

Using these models to measure the luminosity brightening with look-back time, we find, as expected, that the smallest luminosity evolution is measured with the ssp model because the burst of star formation is the shortest of the models that we are considering; conversely, the largest luminosity evolution is measured with the  $\tau = 1.0$  Gyr model because of its extended burst of star formation. For a  $\tau = 0.2$  Gyr model with  $q_o = \frac{1}{2}$ , we find that the theoretical luminosity evolution would be  $\Delta M_{evol}(I) = 0.80$  mag for Cl 1324+3011 at  $z = 0.7565$ ,  $\Delta M_{evol}(I) = 0.99$  mag for Cl

1604+4304 at  $z = 0.8967$ , and  $\Delta M_{evol}(R) = 1.12$  mag for Cl 1604+4321 at  $z = 0.9243$ . These values are  $\sim 0.4$  mag larger in the  $I$  band than what we measure from our analysis (see equation 8). The same difference is found in a comparison between the observations and the models for the brightest cluster galaxy (BCG) in each of our program clusters. On average, the BC96 models predict a BCG magnitude which is  $\sim 0.4$  mag brighter than observed (see §6.1 of PLO01).

If we include the full range of models and cosmologies, the amount of luminosity evolution expressed as the exponent,  $p$ , in  $2.5 \log(1+z)^p$  varies between  $p = 0.85 - 2.36$  in the  $R$  band and  $p = 0.76 - 2.07$  in the  $I$  band, depending on the particular model and  $q_o$ . For a given star-formation model, the amount of evolution increases as  $q_o$  increases. In magnitudes, this luminosity evolution corresponds to  $\Delta M_{evol}(I) = 0.49 - 1.25$  mag for Cl 1324+3011,  $\Delta M_{evol}(I) = 0.53 - 1.44$  mag for Cl 1604+4304, and  $\Delta M_{evol}(R) = 0.61 - 1.68$  mag for Cl 1604+4321.

The results of the theoretical calculations agree well with other measures of luminosity evolution for early-type galaxies at  $z \sim 0.5 - 1$ . Depending on the particular passband and cosmological parameters, the absolute luminosities of field and cluster early-type galaxies are brighter by approximately  $1.0 \pm 0.5$  mag at redshifts of  $z \gtrsim 0.5$  (e.g. Im et al. 1996; Oke, Gunn & Hoessel 1996; Schade et al. 1996, 1999; Smail et al. 1997; van Dokkum et al. 1998; Postman, Lubin & Oke 1998, 2001).

Clearly, the amount of evolution that we require to make  $n = 4$  (see equation 8) is fully consistent, within the errors, with the range of theoretical expectations determined above. Therefore, we assert that we have either (1) detected the evolutionary brightening directly from the  $\langle SB \rangle$  observations on the assumption that the Tolman effect exists, or (2) confirmed that the Tolman test for the reality of the expansion is positive provided that the theoretical luminosity correction for evolution is real.

Our conclusions are fully consistent with the two previous attempts to perform the Tolman Test using primarily ground-based data at more moderate redshifts. Specifically, Sandage & Perlmutter (1991) completed an identical analysis comparing local ellipticals with the first-ranked elliptical galaxies in clusters at redshifts up to  $z \sim 0.6$ . Later, Pahre et al. (1996) used the Kormendy relation between effective radius and mean surface brightness to compare elliptical galaxies in the Coma cluster to those in Abell 2390 ( $z = 0.23$ ) and Abell 851 ( $z = 0.41$ ). Both studies found that the data were fully consistent with the universal expansion assuming simple models of passive evolution of elliptical galaxies.

## 5. Sensitivity of the Conclusions to the Assumption that $q_o = 0$ and $q_o = +1$

We need now to estimate the sensitivity of the results in §3 to the value of  $q_o$ . The sensitivity arises from the differences in the values of the linear radii calculated from the angular radii and the redshift for different values of  $q_o$ . Different linear radii entered into the log R,  $\langle SB \rangle$  diagnostic diagrams of Figures 1 and 2 will give different displacements from the zero-redshift local envelope

lines and, therefore, a different Tolman signal. We can estimate these differences by calculating the change in the linear radii made by changing the value of  $q_o$  and calculating the effect on the Tolman signal using the zero-redshift envelope lines for different  $\eta$  values from Tables 2 and 3 of Paper I.

The Mattig (1958) equations for linear radius  $R = f(q_o, z, H_o)$  and absolute magnitude  $M$  are summarized elsewhere (Sandage 1988; 1995, eqs. 3.9 & 4.5) for any  $q_o$  and arbitrarily large  $z$  values. They will not be repeated here. Table 8 shows the result of using these equations to calculate the necessary parameters for the  $q_o = 0$  and  $+1$  models.

The distance moduli listed in columns 3 and 7 are for  $H_o = 50$ . The log  $A$  values to convert log (angular radii) to log (linear radii) are given in columns 4 and 8 via equations (5) and (6) of §2.1. The differences in absolute magnitude and log R relative to the  $q_o = \frac{1}{2}$  case are listed in columns 5–6 and 9–10 for the  $q_o = 0$  and the  $q_o = +1$  cases, respectively. The magnitude and log R differences relative to the  $q_o = \frac{1}{2}$  case can be used to convert the  $M$ , log R data in Tables 2–4 to the other  $q_o$  cosmologies.

Calculation of the changes in the Tolman signal for different  $q_o$  values is made by multiplying the change in log R from columns 6 and 10 of Table 8 by the slopes in Table 2 of Paper I. These slopes vary between 3.0 and 3.5 depending on the  $\eta$  value. For our most reliable values of  $\eta = 1.7$  and 2.0, the average slope is 3.1. Multiplying the  $\Delta$  Log R values by 3.1 shows that the Tolman signal will be made smaller for the  $q_o = 0$  case relative to that for  $q_o = \frac{1}{2}$ . That is, there will be a smaller deviation from the local line. The required evolutionary correction is made larger by 0.18 mag for Cl 1324+3011 at  $z = 0.7565$ , 0.23 mag for Cl 1604+4304 at  $z = 0.8967$ , and 0.22 mag for Cl 1604+4321 at  $z = 0.9243$ . This difference translates into changing the exponent for the Tolman signal and the evolutionary corrections in equations (7) and (8) for the  $q_o = \frac{1}{2}$  case to  $n = 2.28 \pm 0.17$  and  $4 - n = 1.72 \pm 0.17$  for the  $R$  band and  $n = 3.06 \pm 0.13$  and  $4 - n = 0.94 \pm 0.13$  for the  $I$  band.

The opposite sense is required for the  $q_o = +1$  case because Table 8 shows that the log R values are smaller than for the  $q_o = \frac{1}{2}$  case by  $\{0.057, 0.064, 0.065\}$  dex for  $z = \{0.7565, 0.8967, 0.9243\}$ , respectively. Using smaller log R values in Figures 1 and 2 gives a larger Tolman signal (in magnitudes) by 3.1 times the differences in log R which are listed in Table 8. Consequently, the measured luminosity evolution is smaller by 0.11 mag for Cl 1324+3011 at  $z = 0.7565$ , 0.12 mag for Cl 1604+4304 at  $z = 0.8967$ , and 0.15 mag for Cl 1604+4321 at  $z = 0.9243$ . These changes correspond to a final Tolman signal of  $n = 2.81 \pm 0.17$  and  $n = 3.55 \pm 0.13$  in the  $R$  and  $I$  band, respectively. The corresponding evolutionary requirement is, of course,  $4 - n = 1.19 \pm 0.17$  and  $0.45 \pm 0.13$  for the  $R$  and  $I$  band, respectively.

The conclusion is that the Tolman test as performed here is sensitive to the value of  $q_o$  at the less than 23% level. However, as argued in Paper I, it is not so severe as to make the test degenerate. Our result is that a Tolman signal exists, as modified by evolution, at the level of  $(1 + z)^n$  with  $n$  lying between 2.28 – 2.81 ( $\pm 0.17$ ) in the  $R$  band and between 3.06 – 3.55 ( $\pm 0.13$ )

in the  $I$  band, depending on  $q_o$ . Therefore, the correction for luminosity evolution is  $(1+z)^p$  where  $p$  lies between  $1.72 - 1.19$  ( $\pm 0.17$ ) in the  $R$  band and between  $0.94 - 0.45$  ( $\pm 0.13$ ) in the  $I$  band, again depending on  $q_o$ . The required evolutionary correction to make the real Tolman signal equal to  $(1+z)^4$  is well within the errors of the requirements of Bruzual & Charlot spectral synthesis models, i.e. approximately  $2.5 \log(1+z)^p$  where  $p \approx 0.8$  to  $2.4$  in the  $R$  band and  $p \approx 0.7$  to  $2.1$  in the  $I$  band, as  $q_o$  changes from  $0$  to  $+1$ . Therefore, we conclude that the Tolman prediction is verified and that the expansion is real.

We note that recent studies of high-redshift Type Ia supernovae, the Cosmic Microwave Background, and the statistics of gravitational lenses suggest that the universe is flat with a non-zero cosmological constant,  $\Lambda$  (see e.g. Kochanek 1996; Helbig et al. 1999; de Bernadis et al. 2000; Pryke et al. 2001; Riess et al. 2001 and references therein). Currently, the preferred world model is  $\Omega_M \approx 0.35$  and  $\Omega_\Lambda \approx 0.65$ . In this cosmology, the  $\log R$  values are almost identical to the empty-universe ( $q_o = 0$ ) case; they are larger by only  $0.01$  dex or less at the redshifts of our three clusters. In addition, all flat-universe models with  $0 \leq \Omega_\Lambda \leq 0.65$  give  $\log R$  values which lie within the range that we have calculated for the  $\Omega_\Lambda = 0$  cosmologies (see Table 8). Consequently, our conclusions about the universal expansion are still robust for these  $\Lambda$  cosmologies.

In the next section, we show that the predictions of the “tired light” speculation is not verified at the definitive level of better than  $10 \sigma$ .

## 6. The Tired Light Model Compared with the Observations

In contrast with the standard model with the Mattig equations, there is no metric theory of how distances and magnitudes are measured in a “tired light” model. Therefore, we must guess at a reasonable equation for distance. We adopt a discussion that is given elsewhere (Sandage 1995, §4.3) and use an equation for “coordinate” distance in a flat space which is

$$D = \left( \frac{c}{H_o} \right) \ln(1+z). \quad (12)$$

Because the universe is not expanding in the model, the distance “now” in equation (12) is also the distance when light left. This, of course, is the crucial point. In the expanding case, the distance at the present epoch must be divided by  $(1+z)$  to give the distance when light was emitted. It is this latter distance in the expanding case that, when multiplied by the angular radius, fixes the linear radius.

With  $H_o = 50$ , the linear radius that corresponds to an observed angular radius (in arcsec) in the “tired light” case is

$$\log R(\text{pc}) = 4.464 + \log [\ln(1+z)] + \log \theta'', \quad (13)$$

using equation (12). Hence, the  $A$  term, as defined in equation (5), becomes

$$\log A = 4.464 + \log [\ln(1 + z)]. \quad (14)$$

The  $\log A$  values calculated in this way are listed in column 12 of Table 8 for the three high-redshift clusters. These values, compared with the  $\log A$  values for the  $q_o = \frac{1}{2}$  case, give the increase in the  $\log R$  values that must be entered in the  $\langle SB \rangle$ ,  $\log R$  diagnostic diagram. For example, for Cl 1324+3011 ( $z = 0.7565$ ) the  $\log R$  values must be made larger by 0.305 dex relative to the  $q_o = \frac{1}{2}$  values listed in Table 3.

The magnitudes must also be changed because the distance moduli are different than those in the fiducial  $q_o = \frac{1}{2}$  case. The absolute magnitude calculation for the tired light model follows from the expected theoretical relation that

$$l = \frac{L}{4\pi D^2(1+z)}, \quad (15)$$

where only one power of  $(1+z)$  for the “energy effect” is required, rather than two powers of  $(1+z)$  in the Roberston (1938) equation in the standard theory (cf. Sandage 1995, eq. 2.1). Hence,

$$m - M = 2.5 \log (1 + z) + 5 \log [\ln(1 + z)] + 43.89, \quad (16)$$

for  $H_o = 50$ .

It can be shown from equation (16) that the magnitude–redshift relation for “tired light” is the same to within a few hundredths of a magnitude with the case for  $q_o = +1$  using the Mattig equation. This is true even for redshifts as large as  $z = 1$ . Column 13 of Table 8 confirms this statement, seen by the fact that the entries in column 9 for the  $q_o = +1$  case are very close to those in column 13 for “tired light.” However, these magnitude changes are academic here in using the  $\langle SB \rangle$ ,  $\log R$  diagnostic diagram because no corrections for the magnitude differences need to be applied to the  $\langle SB \rangle$  values. These are *observed*  $\langle SB \rangle$  values (only corrected for  $K$  dimming); hence, as emphasized before, they are independent of all cosmologies.

With the changes to Tables 2–4 for  $\log R$  that are listed in column 14 of Table 8, we can enter Figures 1 and 2 for the “tired light” case in order to measure the depression from the local upper envelope calibration. The result, not shown but which the reader can recover using the  $\Delta \log R$  values given in Table 8 together with Tables 2–4, is that a measurable  $\langle SB \rangle$  depression at these larger  $\log R$  values is again present. It is, of course, smaller than for the expanding case because of the larger  $\log R$  values. But, by how much? The crucial question is whether it is so much smaller as to conform to a depression of only  $2.5 \log (1 + z)$  mag when the correction for luminosity evolution is also applied.

We have analyzed the data for the three clusters in the same way as in §3; however, we now use the correct  $\log R$  values required by the “tired light” conjecture, using the recipes in Table 8. Expressing the result of the  $\langle SB \rangle$  depression from the zero-redshift fiducial line in the  $\langle SB \rangle$ ,  $\log R$  diagram as the exponent,  $n$ , in  $2.5 \log(1+z)^n$  gives the weighted mean of  $n = 1.61 \pm 0.13$  for the  $R$  band and  $n = 2.27 \pm 0.12$  for the  $I$  band. As described in §3, we have used the results from the most reliable  $\eta$  values of  $\eta = 1.7$  and  $2.0$ . The resulting exponents are *too large* by approximately 5 and 10  $\sigma$ , respectively, compared to the  $n = 1$  prediction of the “tired light” scenario. Consequently, to produce coherence with the “tired light” model, we require negative luminosity evolution in the look-back time, i.e. *galaxies must be fainter in the past*. No feasible model of stellar evolution can produce such luminosity evolution with time.

In fact, just as in the expanding case, positive luminosity evolution must have occurred in the look-back time because there is no way in the tired light model to prevent the stellar content of galaxies from evolving during the look-back time.

A static model where the redshift is not due to expansion is not the same as a steady state model where the mean parameters of galaxies, averaged over an ensemble of galaxies, are required to be the same at all distances and at all times. For a steady state to exist, despite the evolution of the stellar content of individual galaxies, requires that there must be young and old galaxies in every volume of space and at every cosmic time such that the mean age is the same at all distances and times. This requires continuous galaxy formation at the same rate at all cosmic times in order to maintain a constant mean age everywhere, always.

However, such steady state models are not the same as static models where the redshift is due to an unknown physical cause, either at the source or in the intervening light path from the source to the observer as originally postulated by Zwicky (1929). In fact, the steady state models proposed by Bondi, Gold, and Hoyle are truly expanding models where the redshift is due to the expansion. They are not static models. Furthermore, an early proof that steady state models cannot be correct was the demonstration of the failure of the predicted steady state color distribution, with its required mixture of ages, to match the observed color distribution of early-type galaxies (Sandage 1973).

Hence, as in the present paper, evolutionary corrections to magnitudes must be applied to both the expanding and the static models in making the present test. The supposed degeneracy of the Tolman test due to the identity claimed by Moles et al. (1998) of the surface brightness effect in both the expanding and a static (tired light) case is not correct. Their error is due to a category mistake by confusing static and steady-state models. What Moles et al. have done is to combine a static model with a steady state model. This is a higher order departure from the standard expanding model than we have considered here and is not the test we have made. In any case, as stated above, a steady state model can again be disproved by the color argument (Sandage 1973). Hence, even the higher order model proposed by Moles et al. cannot be correct on this ground alone.

The result of the present paper is that a static model, where the redshift is due to an unknown physical cause, fails the surface brightness test by a large factor. Such a model requires luminosity evolution in the look-back time, just as in the expanding case. Based on the analysis in §4, we find that a good approximation for the amount of increase in luminosity at the epoch of light emission is  $2.5 \log(1+z)^p$  mag, where  $p > 0.7$ . Applying this correction to the “tired light” analysis gives the intrinsic “tired light” prediction for the corrected exponents of  $> 2.31 (\pm 0.13)$  and  $> 2.87 (\pm 0.12)$  for the  $R$  and  $I$  bands, respectively. Each value is more than  $10 \sigma$  from the required exponent of 1.0 if the “tired light” scenerio were correct. We take this to be a definitive proof that the hypothesis of non-expansion does not fit the surface brightness data.

## 7. Systematic Uncertainties in the Experiment : How can the Present Result be Improved?

There are two systematic uncertainties in the present experiment. Although neither of them are severe enough to jeopardize the results presented in §3 and §5 that the expansion is real, each can be overcome by more data with expanded boundary conditions on the parameters compared to the data used here.

First, the principal uncertainty at small radii ( $\log R < 4.0$ ) is the position of the zero-redshift fiducial line in the  $\langle SB \rangle$ ,  $\log R$  diagram, relative to which the  $\langle SB \rangle$  depressions for high-redshift galaxies are compared. The Postman & Lauer (1995) data (Figure 2 of Paper I) do not extend to radii smaller than  $\log R(\text{pc}) = 4.0$ . Their data are confined to the first ranked cluster early-type galaxies. They do not sample into the luminosity function of each cluster to provide data for smaller galaxies. We have extended the data to smaller radii with the sample in Sandage & Perelmuter (1991) to generate a non-linear correction at small radii to the best-fit linear equations to the Postman & Lauer (1995) data (see Table 3 of Paper I). However, the Sandage & Perelmuter (1991) data are also only for the first few, brightest cluster galaxies, again not going far into the fainter part of the luminosity function. Hence, although Table 3 of Paper I gives our adopted extension to radii as small as  $\log R(\text{pc}) = 3.3$ , the uncertainties are large and can be reduced by a more complete study of the  $\langle SB \rangle$ ,  $\log R$  relation for fainter and smaller galaxies at low redshift.

Second, the three clusters studied here are near the faint end of the distribution of absolute magnitude of first ranked galaxies in, for example, the sample of first ranked cluster galaxies whose data are listed by Kristian, Sandage & Westphal (1978). The mean of the distribution of absolute magnitude in the  $R$  band for the Kristian et al. sample is  $\langle M_R \rangle = -24.5$ , whereas the first-ranked early-type galaxies in the three clusters studied have absolute magnitudes of  $M_R = -23.7$  for Cl 1604+4321,  $-23.7$  for Cl 1604+4304, and  $-24.2$  for Cl 1324+3011 (see PLO01). (Note again that the system of  $R_J$  magnitudes used by Kristian et al. is 0.25 mag brighter than the Cape  $R$  system used here). The galaxies in the three clusters studied here have fainter absolute magnitudes and smaller radii than the average local clusters, exacerbating the problem described above. Richer high-redshift clusters with brighter and, therefore, larger first-ranked galaxies are known. A study

of the HST data from such clusters will improve the present Tolman test. We suspect that the present experiment is only the beginning of similar work that will be done in the coming years with HST on such clusters as they are discovered and observed.

We are grateful to Mark Postman and J.B. Oke for their permission to use part of their extensive Keck and HST database for this paper and the previous papers in the series. LML would like to thank Chris Fassnacht for his essential material aids to this paper. AS is grateful for a conversation with James Peebles concerning the proof of the Tolman  $(1+z)^4$  factor from the exact normalization of the observed Planck black body background radiation in the COBE experiment, as discussed in §1.4.3.

LML was supported through Hubble Fellowship grant HF-01095.01-97A from the Space Telescope Science Institute, which is operated by the Associated Universities for Research in Astronomy, Inc. under NASA contract NAS 5-26555. AS acknowledges support for publication from NASA grants GO-5427.01-93A and G-06459.01-95A for work that is related to data taken with the *Hubble Space Telescope*.

## REFERENCES

- Aragón-Salamanca, A., Ellis, R.S., Couch, W.J., & Carter, D. 1993, MNRAS, 262, 764
- Baade, W. 1938, ApJ, 88, 285
- Bahcall, J.N. & Wolf, R.A. 1968, ApJ, 152, 701
- Bergbush, P.A. & VandenBerg, D.A. 1992, ApJS, 81, 163
- Bruzual, A.G. & Charlot, S. 1993, ApJ, 405, 538
- Cowie, L.L, Gardner, J.P., Hu, E.M., Songaila, A., Hodapp, K.-H., & Wainscoat, P.J. 1994, Nature, 371, 43
- de Bernardis, P. et al. 2000, Nature, 404, 955
- de Propis, R., Stanford, S.A., Eisenhardt, P.R., Dickinson, M., & Elston, R. 1999, AJ, 118, 719
- de Sitter, W. 1917a, Proc. Akad. Wetensch. Amsterdam, 19, 1217
- de Sitter, W. 1917b, MNRAS, 78, 3
- de Sitter, W. 1933, The Astronomical Aspect of the Theory of Relativity, University of California Pub. in Mathematics (Berkeley: Univ. Calif. Press), Vol. 2, No. 8
- Eddington, A.S. 1923, Mathematical Theory of Relativity, (Cambridge, Cambridge University Press)
- Ellis, R.S., Smail, I., Dressler, A., Couch, W.A., Oemler, A., Butcher, H., & Sharples, R.M. 1997, ApJ, 483, 582
- Fixsen, D.J., Cheng, E.S., Gales, J.M., Mather, J.C., Shafer, R.A., & Wright, E.L. 1996, ApJ, 473, 576
- Friedmann, A.A. 1922, Zs. f. Phys., 10, 377
- Ge, J., Bechtold, J., & Black, J.H. 1997, ApJ, 474, 67
- Goldhaber, G. et al. 1997, in Thermonuclear Supernovae, eds. R. Canal, P. Ruiz-Lapuente, & J. Isern (Dordrecht: Kluwer), 777
- Goldhaber, G. et al. 2001, ApJ, submitted
- Guiderdoni, B., & Rocca-Volmerange, B. 1987, A&A, 186, 1
- Guiderdoni, B., & Rocca-Volmerange, B. 1988, A&AS, 74, 185
- Helbig, P., marlow, D., Quast, R., Wilkinson, P.N., Browne, I.W.A., & Koopmans, L.V.E. 1999, A&AS, 136, 297

- Hoyle, F. & Sandage, A. 1956, PASP, 68, 301
- Hubble, E. 1925, ApJ, 62, 409 (NGC 6822)
- Hubble, E. 1926, ApJ, 63, 236 (M33)
- Hubble, E. 1929a, Proc. Nat. Acad. Sci., 15, 168
- Hubble, E. 1929b, ApJ, 69, 103 (M31)
- Hubble, E. 1934, ApJ, 79, 8
- Hubble, E. 1936a, ApJ, 84, 270
- Hubble, E. 1936b, ApJ, 84, 517
- Hubble, E. 1953, MNRAS, 113, 658
- Hubble, E. & Humason, M.L. 1931, ApJ, 74, 43
- Humason, M.L. 1929, Proc. Nat. Acad. Sci., 15, 167
- Humason, M.L. 1936, ApJ, 83, 10.
- Im, M., Griffiths, R.E., Ratnatunga, K.U., & Sarajedini, V.L. 1996, ApJ, 461, L79
- Kochanek, C.S. 1996, ApJ, 466, 638
- Kristian, J.M., Sandage, A., & Westphal, J. 1978, ApJ, 221, 383
- La Violette, P.A. 1986, ApJ, 301, 544
- Lemaitre, G. 1927, Ann. Soc. Sci. Bruxelles, 47A, 49
- Lemaitre, G. 1931, MNRAS, 91, 483 (the 1927 paper in English translation)
- Lubin, L.M. & Sandage, A. 2001a, AJ, 121, 2289 (Paper II)
- Lubin, L.M. & Sandage, A. 2001b, AJ, in press (Paper III)
- Lubin, L.M., Postman, M., Oke, J.B., Ratnatunga, K.U., Gunn, J.E., Hoessel, J.G., & Schneider, D.P. 1998, AJ, 116, 584
- Lubin, L.M., Postman, M., Oke, J.B., Brunner, R., Gunn, J.E., & Schneider, D.P. 2001, AJ, in preparation
- Lundmark, K. 1925, MNRAS, 85, 865
- Mather, J.C. et al. 1990, ApJ, 354, L37

- Mattig, W. 1958, *Astron. Nach.*, 284, 109
- Mattig, W. 1959, *Astron. Nach.*, 285, 1
- Meyer, D.M., Black, J.H., Chafee, F.H., Foltz, G., & York, D. 1986, *ApJ*, 308, L37
- Minkowski, R. 1964, *ARAA*, 2, 247
- Moles, M., Campos, A., Kjaergaard, P., Fasano, G., & Belloni, D. 1998, *ApJ*, 495, L34
- Oke, J. B., Gunn, J.E., & Hoessel, J.G. 1996, *AJ*, 111, 290.
- Oke, J.B., Postman, M., & Lubin, L.M. 1998, *AJ*, 116, 549 (OPL)
- Pahre, M.A., Djorgovski, S.G., & de Carvalho, R.R. 1996, *ApJ*, 456, L79
- Parodi, B.R., Saha, A., Sandage, A., & Tammann, G.A. 2000, *ApJ*, 540, 634
- Pecker, J.-C. & Vigier, J.-P. 1987, in *Observational Cosmology*, IAU Symp. 124, eds. A. Hewitt, G. Burbidge, & L-A. Fang (Dordrecht: Reidel), 50
- Petrosian, V. 1976, *ApJ*, 209, L1
- Postman, M. & Lauer, T. 1995, *ApJ*, 440, 28
- Postman, M., Lubin, L.M., & Oke, J.B. 1998, *AJ*, 116, 560 (PLO98)
- Postman, M., Lubin, L.M., & Oke, J.B. 2001, *AJ*, in press (PLO01)
- Poulain, P. & Nieto, J.-L. 1994, *A&AS*, 103, 573
- Pryke, C., Halverson, N.W., Leitch, E.M., Kovac, J., Carlstrom, J.E., Holzzapfel, W.L., & Dragovan, M. 2001, *ApJ*, submitted
- Riess, A.G. et al. 2001, *ApJ*, in press
- Robertson, H.P. 1928, *Phil. Mag.*, 5, 835
- Robertson, H.P. 1938, *Zs. f. Ap*, 15, 69
- Rocca-Volmerange, B. & Guiderdoni, B. 1988, *A&AS*, 75, 93
- Saha, A., Sandage, A., Tammann, G.A., Labhardt, L., Macchetto, F.D., & Panagia, N. 1999, *ApJ*, 522, 802
- Salpeter, E.E. 1955, *ApJ*, 121, 161
- Sandage, A. 1961a, *ApJ*, 133, 355
- Sandage, A. 1961b, *ApJ*, 134, 916

- Sandage, A. 1973, *ApJ*, 183, 711
- Sandage, A. 1975, in *Galaxies and the Universe*, eds. A. Sandage, M. Sandage, & G. Kristian, (Chicago : Univ. Chicago Press), Chapter 19
- Sandage, A. 1988, *ARAA*, 26, 561
- Sandage, A. 1993, *AJ*, 106, 7191
- Sandage, A. 1995, “Practical Cosmology: Inventing the Past,” in *The Deep Universe*, 23rd Sass Fee Advanced Course in Astrophysics, eds. B. Binggeli & R. Buser (Springer: Berlin)
- Sandage, A. 1997, *PASP*, 109, 1193
- Sandage, A. 1998, in *The Hubble Deep Field*, Space Telescope Science Institute Symposium Series No. 11, eds. M. Livio, S.M. Fall, & P. Madau, (Cambridge: Cambridge University Press), 1
- Sandage, A. 1999, *ApJ*, 527, 479
- Sandage, A. & Perelmuter, J.-M. 1991, *ApJ*, 370, 455
- Sandage, A. & Tammann, G.A. 1997, in *Critical Dialogues in Cosmology*, ed. N. Turok, (Singapore : World Scientific), 130
- Sandage, A., & Lubin, L.M. 2001, *AJ*, 121, 2271 (Paper I)
- Scalo, L.M. 1986, *Fund Cosmic Phys*, 11, 1
- Schade, D., Carlberg, R.G., Yee, H.K.C., & López-Cruix, O. 1996, *ApJ*, 646, L63
- Schade, D. et al. 1999, *ApJ*, 525, 31
- Silberstein, L. 1924, *MNRAS*, 84, 365
- Smail, I., Dressler, A., Couch, W.J., Ellis, R.S., Oemler, A., Butcher, H., & Sharples, R.M. 1997, *ApJS*, 110, 213
- Songaila, A. et al. 1994, *Nat*, 371, 43
- Srianand, R., Petitjean, P. & Ledoux, C. 200, *Nat*, 408, 931
- Stanford, S.A., Eisenhardt, P.R., & Dickinson, M. 1995, *ApJ*, 450, 512
- Stanford, S.A., Eisenhardt, P.R., & Dickinson, M. 1998, *ApJ*, 492, 461.
- Stromberg, G. 1925, *ApJ*, 61, 353
- Theureau, G., Harrski, M., Ekholm, T., Bottinelli, L., Gouguenheim, L., Palurel, G., & Teerikorpi, P. 1997, *A&A*, 322, 730

- Tinsley, B.M. 1968, *ApJ*, 151, 547
- Tinsley, B.M. 1972a, *ApJL*, 173, L93
- Tinsley, B.M. 1972b, *A&A*, 20, 383
- Tinsley, B.M. 1976, *ApJ*, 203, 63
- Tinsley, B.M. 1977, *ApJ*, 211, 621
- Tinsley, B.M. 1980, *ApJ*, 241, 41
- Tolman, R.C. 1929, *Proc. Nat. Acad. Sci.*, 15, 297
- Tolman, R.C. 1930, *Proc. Nat. Acad. Sci.*, 16, 511
- Tolman, R.C. 1934, *Relativity, Thermodynamics, and Cosmology*, (Oxford: Oxford University Press)
- Tropp, E.A., Frenkel, V. Ya., & Chernin, A.D. 1993, in Alexander A. Friedmann, (Cambridge: Cambridge University Press)
- van Dokkum, P., Franx, M., Kelson, D., & Illingworth, G. 1998, *ApJ*, 504, L17
- Wilson, O.C. 1939, *ApJ*, 90, 634
- Wirtz, C. 1925, *Scientia*, 38, 303
- Worthey, G. 1994, *ApJS*, 95, 107
- Zwicky, F. 1929, *Proc. Nat. Acad. Sci.*, 15, 773
- Zwicky, F. 1957, *Morphological Astronomy*, (Berlin: Springer)

Table 1. Adopted  $K$ -corrections, Distance Moduli, and  $A$  Factor for the Linear Radii using  $q_o = \frac{1}{2}$ ,  $H_o = 50$

Cluster	$z$	$K(R) \pm \Delta K(R)$ (mag)	$K(I) \pm \Delta K(I)$ (mag)	$m - M$	$\log A$
1324+3011	0.7565	...	$0.71 \pm 0.03$	43.57	3.910
1604+4304	0.8967	...	$0.80 \pm 0.07$	43.97	3.924
1604+4321	0.9243	$1.89 \pm 0.06$	...	44.04	3.926

Table 2. The  $M$ ,  $\langle SB \rangle$ , Log R Data for Cl 1604+4321 [ $R$  Band;  $q_o = \frac{1}{2}$ ;  $H_o = 50$ ]

Gal #	$\eta = 1.0$			$\eta = 1.3$			$\eta = 1.5$			$\eta = 1.7$			$\eta = 2.0$		
	$M^a$	$\langle SB \rangle^a$	Log R(pc)	$M^a$	$\langle SB \rangle^a$	Log R(pc)	$M^a$	$\langle SB \rangle^a$	Log R(pc)	$M^a$	$\langle SB \rangle^a$	Log R(pc)	$M^a$	$\langle SB \rangle^a$	Log R(pc)
23 <sup>b</sup>	$-23.13 \pm 0.10$	18.48	3.224	$-23.46 \pm 0.09$	19.16	3.409	$-23.57 \pm 0.09$	19.49	3.493	$-23.65 \pm 0.08$	19.81	3.571	$-23.78 \pm 0.08$	20.48	3.729
29 <sup>b</sup>	$-23.11 \pm 0.10$	20.35	3.568	$-23.28 \pm 0.09$	20.71	3.674	$-23.37 \pm 0.09$	20.97	3.742	$-23.44 \pm 0.08$	21.23	3.805	$-23.56 \pm 0.08$	21.84	3.955
36	$-22.46 \pm 0.10$	20.24	3.420	$-22.82 \pm 0.09$	20.97	3.632	$-22.94 \pm 0.08$	21.34	3.727	$-23.05 \pm 0.08$	21.74	3.809	$-23.15 \pm 0.08$	22.28	3.966
38	$-22.63 \pm 0.10$	20.21	3.451	$-22.87 \pm 0.09$	20.71	3.583	$-22.97 \pm 0.08$	21.02	3.666	$-23.06 \pm 0.08$	21.39	3.767	$-23.20 \pm 0.08$	22.02	3.918
44 <sup>b</sup>	$-22.47 \pm 0.09$	21.06	3.586	$-22.84 \pm 0.09$	21.76	3.790	$-22.95 \pm 0.09$	22.10	3.881	$-23.04 \pm 0.08$	22.40	3.959	$-23.12 \pm 0.08$	22.82	4.058
46	$-22.30 \pm 0.10$	21.20	3.581	$-22.63 \pm 0.09$	21.89	3.778	$-22.77 \pm 0.08$	22.27	3.879	$-22.86 \pm 0.08$	22.62	3.966	...	...	...
49	$-21.95 \pm 0.10$	20.07	3.303	$-22.56 \pm 0.09$	21.33	3.647	$-22.71 \pm 0.09$	21.77	3.770	$-22.80 \pm 0.08$	22.10	3.853	$-22.88 \pm 0.08$	22.46	3.930
57	$-22.15 \pm 0.10$	21.65	3.636	$-22.58 \pm 0.09$	22.50	3.887	$-22.79 \pm 0.09$	23.05	4.029	$-22.88 \pm 0.08$	23.39	4.132	$-22.92 \pm 0.08$	23.58	4.171
58	$-21.88 \pm 0.10$	20.38	3.345	$-22.24 \pm 0.09$	21.11	3.547	$-22.45 \pm 0.09$	21.72	3.707	$-22.67 \pm 0.08$	22.54	3.913	$-22.82 \pm 0.08$	23.25	4.083
65	$-22.10 \pm 0.10$	19.83	3.278	$-22.40 \pm 0.09$	20.44	3.441	$-22.50 \pm 0.08$	20.74	3.515	$-22.57 \pm 0.08$	21.01	3.590	$-22.64 \pm 0.08$	21.43	3.667
78 <sup>b</sup>	$-21.53 \pm 0.10$	20.70	3.336	$-21.86 \pm 0.09$	21.40	3.529	$-22.00 \pm 0.09$	21.80	3.643	$-22.14 \pm 0.08$	22.30	3.759	$-22.17 \pm 0.08$	22.48	3.801
112 <sup>b</sup>	$-21.29 \pm 0.10$	20.27	3.219	$-21.60 \pm 0.09$	20.94	3.383	$-21.70 \pm 0.08$	21.27	3.477	$-21.79 \pm 0.08$	21.62	3.568	$-21.89 \pm 0.08$	22.12	3.667
115 <sup>b</sup>	$-21.16 \pm 0.09$	21.09	3.325	$-21.55 \pm 0.10$	21.87	3.556	$-21.64 \pm 0.08$	22.14	3.618	$-21.71 \pm 0.08$	22.44	3.718	$-21.84 \pm 0.08$	22.95	3.860
144 <sup>b</sup>	$-21.01 \pm 0.10$	20.74	3.246	$-21.37 \pm 0.09$	21.49	3.461	$-21.48 \pm 0.09$	21.82	3.536	$-21.58 \pm 0.08$	22.21	3.632	$-21.69 \pm 0.08$	22.78	3.767

<sup>a</sup>Values have been corrected with the appropriate  $K(R) = 1.89$  correction (see Table 1).

<sup>b</sup>Member galaxy selected based on its photometric redshift (see Brunner & Lubin 2000).

Table 3. The  $M$ ,  $\langle SB \rangle$ , Log R Data for Cl 1324+3011 [ $I$  Band;  $q_o = \frac{1}{2}$ ;  $H_o = 50$ ]

Gal #	$\eta = 1.0$			$\eta = 1.3$			$\eta = 1.5$			$\eta = 1.7$			$\eta = 2.0$		
	$M^a$	$\langle SB \rangle^a$	Log R(pc)	$M^a$	$\langle SB \rangle^a$	Log R(pc)	$M^a$	$\langle SB \rangle^a$	Log R(pc)	$M^a$	$\langle SB \rangle^a$	Log R(pc)	$M^a$	$\langle SB \rangle^a$	Log R(pc)
9	$-23.23 \pm 0.07$	19.11	3.425	$-24.03 \pm 0.05$	20.75	3.905	$-24.46 \pm 0.04$	21.87	4.294	...	...	...	...	...	...
11	$-23.21 \pm 0.07$	19.89	3.574	$-23.87 \pm 0.05$	21.21	3.964	$-24.11 \pm 0.04$	21.82	4.136	$-24.18 \pm 0.04$	22.04	4.222	...	...	...
12	$-23.31 \pm 0.06$	20.27	3.667	$-23.54 \pm 0.05$	20.73	3.802	$-23.63 \pm 0.05$	20.97	3.866	$-23.68 \pm 0.04$	21.15	3.915	$-23.73 \pm 0.04$	21.39	3.968
18	$-22.69 \pm 0.07$	19.65	3.424	$-23.05 \pm 0.05$	20.39	3.638	$-23.20 \pm 0.05$	20.81	3.749	$-23.32 \pm 0.05$	21.24	3.859	$-23.46 \pm 0.04$	21.95	4.029
21	$-22.45 \pm 0.08$	19.36	3.327	$-22.91 \pm 0.06$	20.31	3.603	$-23.08 \pm 0.05$	20.81	3.734	$-23.20 \pm 0.05$	21.26	3.843	$-23.29 \pm 0.04$	21.69	3.952
26	$-22.24 \pm 0.07$	20.20	3.446	$-22.88 \pm 0.05$	21.44	3.816	$-23.02 \pm 0.05$	21.82	3.912	$-23.12 \pm 0.05$	22.16	3.995	$-23.17 \pm 0.04$	22.41	4.070
29	$-22.47 \pm 0.06$	20.36	3.519	$-22.83 \pm 0.05$	21.08	3.742	$-23.00 \pm 0.04$	21.55	3.851	$-23.25 \pm 0.04$	22.45	4.087	$-23.32 \pm 0.04$	22.81	4.174
30 <sup>b</sup>	$-22.42 \pm 0.07$	20.52	3.546	$-22.61 \pm 0.05$	20.93	3.657	$-22.72 \pm 0.05$	21.22	3.740	$-22.82 \pm 0.04$	21.62	3.841	$-22.89 \pm 0.04$	21.95	3.918
40	$-21.78 \pm 0.07$	19.42	3.229	$-22.19 \pm 0.05$	20.28	3.447	$-22.37 \pm 0.05$	20.81	3.588	$-22.49 \pm 0.04$	21.28	3.702	$-22.58 \pm 0.04$	21.72	3.811
55 <sup>b</sup>	$-21.43 \pm 0.07$	20.50	3.348	$-21.69 \pm 0.05$	21.04	3.502	$-21.78 \pm 0.05$	21.31	3.571	$-21.83 \pm 0.04$	21.52	3.619	$-21.91 \pm 0.03$	21.94	3.710
59	$-21.60 \pm 0.08$	19.73	3.245	$-21.89 \pm 0.05$	20.30	3.395	$-21.99 \pm 0.04$	20.57	3.465	$-22.04 \pm 0.04$	20.81	3.526	$-22.11 \pm 0.04$	21.16	3.605
69	$-21.48 \pm 0.04$	19.24	3.109	$-21.71 \pm 0.06$	19.76	3.256	$-21.80 \pm 0.04$	20.05	3.327	$-21.86 \pm 0.04$	20.29	3.382	$-21.92 \pm 0.03$	20.61	3.455
74 <sup>b</sup>	$-21.27 \pm 0.07$	21.28	3.470	$-21.57 \pm 0.05$	21.91	3.648	$-21.72 \pm 0.05$	22.34	3.764	$-21.92 \pm 0.04$	23.03	3.938	$-21.99 \pm 0.04$	23.35	4.016

<sup>a</sup>Values have been corrected with the appropriate  $K(I) = 0.71$  correction (see Table 1).

<sup>b</sup>Member galaxy selected based on its photometric redshift (see Brunner & Lubin 2000).

Table 4. The  $M$ ,  $\langle SB \rangle$ , Log R Data for Cl 1604+4304 [ $I$  Band;  $q_o = \frac{1}{2}$ ;  $H_o = 50$ ]

Gal #	$\eta = 1.0$			$\eta = 1.3$			$\eta = 1.5$			$\eta = 1.7$			$\eta = 2.0$		
	$M^a$	$\langle SB \rangle^a$	Log R(pc)	$M^a$	$\langle SB \rangle^a$	Log R(pc)	$M^a$	$\langle SB \rangle^a$	Log R(pc)	$M^a$	$\langle SB \rangle^a$	Log R(pc)	$M^a$	$\langle SB \rangle^a$	Log R(pc)
9	$-23.24 \pm 0.10$	20.59	3.651	$-23.72 \pm 0.10$	21.55	3.938	$-23.89 \pm 0.09$	22.03	4.062	$-23.98 \pm 0.09$	22.36	4.149	$-24.04 \pm 0.09$	22.59	4.204
10 <sup>b</sup>	$-23.12 \pm 0.10$	20.90	3.687	$-23.59 \pm 0.10$	21.82	3.963	$-23.71 \pm 0.09$	22.16	4.058	$-23.80 \pm 0.09$	22.46	4.131	...	...	...
13	$-23.17 \pm 0.10$	20.00	3.525	$-23.41 \pm 0.10$	20.50	3.669	$-23.51 \pm 0.09$	20.80	3.746	$-23.59 \pm 0.09$	21.10	3.821	$-23.68 \pm 0.09$	21.53	3.924
34 <sup>b</sup>	$-22.06 \pm 0.10$	20.98	3.495	$-22.35 \pm 0.09$	21.60	3.674	$-22.50 \pm 0.09$	22.03	3.785	$-22.58 \pm 0.09$	22.32	3.866	$-22.64 \pm 0.09$	22.60	3.930
46 <sup>b</sup>	$-22.01 \pm 0.11$	20.40	3.378	$-22.25 \pm 0.10$	20.90	3.513	$-22.34 \pm 0.09$	21.17	3.589	$-22.42 \pm 0.09$	21.46	3.661	$-22.50 \pm 0.09$	21.90	3.761
50	$-21.83 \pm 0.11$	21.11	3.479	$-22.18 \pm 0.10$	21.83	3.689	$-22.39 \pm 0.09$	22.43	3.855	$-22.47 \pm 0.09$	22.73	3.919	$-22.60 \pm 0.09$	23.38	4.077
58 <sup>b</sup>	$-21.72 \pm 0.10$	20.65	3.371	$-21.94 \pm 0.09$	21.11	3.499	$-22.03 \pm 0.09$	21.37	3.569	$-22.10 \pm 0.09$	21.63	3.632	$-22.18 \pm 0.09$	22.03	3.725

<sup>a</sup>Values have been corrected with the appropriate  $K(I) = 0.80$  correction (see Table 1).

<sup>b</sup>Member galaxy selected based on its photometric redshift (see Brunner & Lubin 2000).

Table 5. Summary of the Tolman Signal and the Inferred Luminosity Evolution for Cl 1604+4321 in the  $R$  band using  $q_o = \frac{1}{2}$

$\eta$	$\Delta\langle SB \rangle$ (mag)	$n$	$\Delta M_{evol}$ (mag)	$4 - n$	#
(1)	(2)	(3)	(4)	(5)	(6)
1.0	$2.44 \pm 0.16$	$3.43 \pm 0.23$	$0.40 \pm 0.16$	$0.57 \pm 0.23$	14
1.3	$2.24 \pm 0.16$	$3.15 \pm 0.23$	$0.60 \pm 0.16$	$0.85 \pm 0.23$	14
1.5	$2.21 \pm 0.16$	$3.11 \pm 0.23$	$0.63 \pm 0.16$	$0.89 \pm 0.23$	14
1.7	$1.96 \pm 0.17$	$2.76 \pm 0.24$	$0.88 \pm 0.17$	$1.24 \pm 0.24$	14
2.0	$1.76 \pm 0.18$	$2.48 \pm 0.25$	$1.08 \pm 0.18$	$1.52 \pm 0.25$	13

Table 6. Summary of the Tolman Signal and the Inferred Luminosity Evolution for Cl 1324+3011 in the  $I$  band using  $q_o = \frac{1}{2}$

$\eta$	$\Delta\langle SB \rangle$ (mag)	$n$	$\Delta M_{evol}$ (mag)	$4 - n$	#
(1)	(2)	(3)	(4)	(5)	(6)
1.0	$2.54 \pm 0.15$	$4.15 \pm 0.25$	$-0.09 \pm 0.15$	$-0.15 \pm 0.25$	13
1.3	$2.33 \pm 0.14$	$3.81 \pm 0.23$	$0.12 \pm 0.14$	$0.19 \pm 0.23$	13
1.5	$2.33 \pm 0.13$	$3.81 \pm 0.21$	$0.12 \pm 0.13$	$0.19 \pm 0.21$	13
1.7	$2.13 \pm 0.14$	$3.48 \pm 0.23$	$0.32 \pm 0.14$	$0.52 \pm 0.23$	12
2.0	$1.99 \pm 0.15$	$3.25 \pm 0.25$	$0.46 \pm 0.15$	$0.75 \pm 0.25$	11

Table 7. Summary of the Tolman Signal and the Inferred Luminosity Evolution for Cl 1604+4304 in the  $I$  band using  $q_o = \frac{1}{2}$

$\eta$	$\Delta\langle SB \rangle$ (mag)	$n$	$\Delta M_{evol}$ (mag)	$4 - n$	#
(1)	(2)	(3)	(4)	(5)	(6)
1.0	$2.92 \pm 0.18$	$4.20 \pm 0.26$	$-0.14 \pm 0.18$	$-0.20 \pm 0.26$	7
1.3	$2.73 \pm 0.17$	$3.93 \pm 0.24$	$0.05 \pm 0.17$	$0.07 \pm 0.24$	7
1.5	$2.72 \pm 0.17$	$3.91 \pm 0.24$	$0.06 \pm 0.17$	$0.08 \pm 0.24$	7
1.7	$2.43 \pm 0.18$	$3.50 \pm 0.26$	$0.35 \pm 0.18$	$0.50 \pm 0.26$	7
2.0	$2.29 \pm 0.21$	$3.29 \pm 0.30$	$0.49 \pm 0.21$	$0.71 \pm 0.30$	6

Table 8. Recipes to Convert the  $q_o = \frac{1}{2}$ ,  $H_o = 50$  Tables for Log R and  $m - M$  to the Other Cosmologies

Cluster (1)	$z$ (2)	$m - M$ (3)	Log $A$ (4)	$q_o = 0$		$m - M$ (7)	Log $A$ (8)	$q_o = 1$		$m - M$ (11)	"Tired Light"		$\Delta$ Log R (14)
				$\Delta M$ (5)	$\Delta$ Log R (6)			$\Delta M$ (9)	$\Delta$ Log R (10)		Log $A$ (12)	$\Delta M$ (13)	
Cl 1324+3011	0.7565	43.98	3.992	0.41 brighter	0.082 larger	43.28	3.853	0.29 fainter	0.057 smaller	43.26	4.215	0.31 fainter	0.305 larger
Cl 1604+4304	0.8967	44.46	4.021	0.49 brighter	0.097 larger	43.66	3.860	0.31 fainter	0.064 smaller	43.62	4.270	0.35 fainter	0.346 larger
Cl 1604+4321	0.9243	44.53	4.025	0.50 brighter	0.100 larger	43.73	3.861	0.32 fainter	0.065 smaller	43.68	4.280	0.36 fainter	0.354 larger

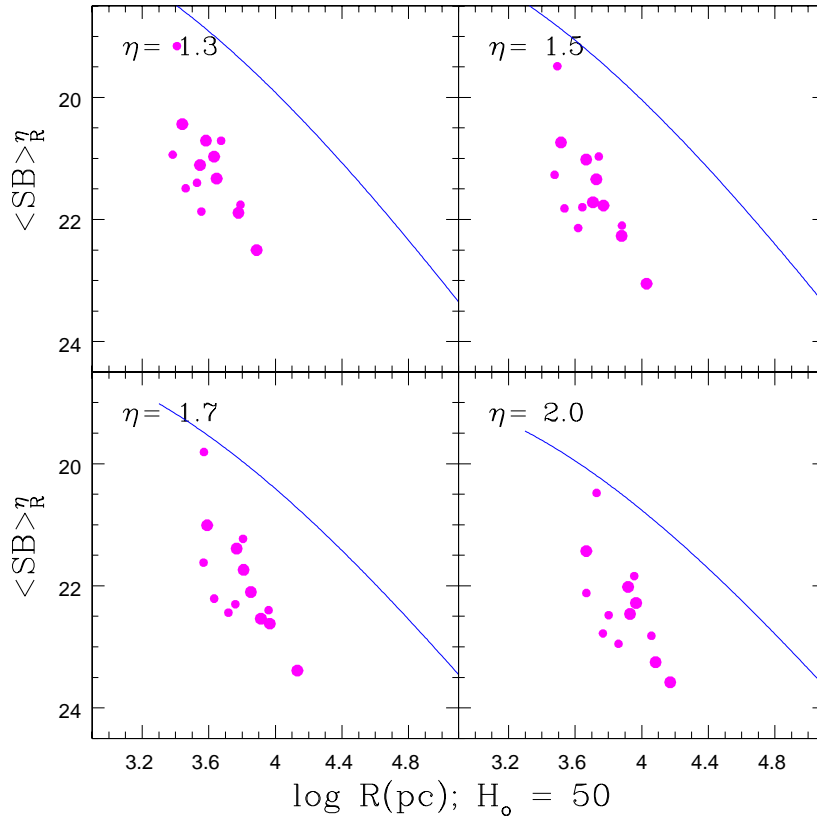


Fig. 1.— Surface brightness measured in the  $R$  band versus log linear radius for the galaxies in Cl 1604+4321 ( $z = 0.9243$ ) from the data in Table 2. Large dots are for the galaxies in Table 2 with directly measured redshifts. Small dots are cluster members inferred for their photometric redshifts (see Paper III). The mean correlation for zero-redshift early-type galaxies is shown by the lines taken from Tables 2 and 3 of Paper I.

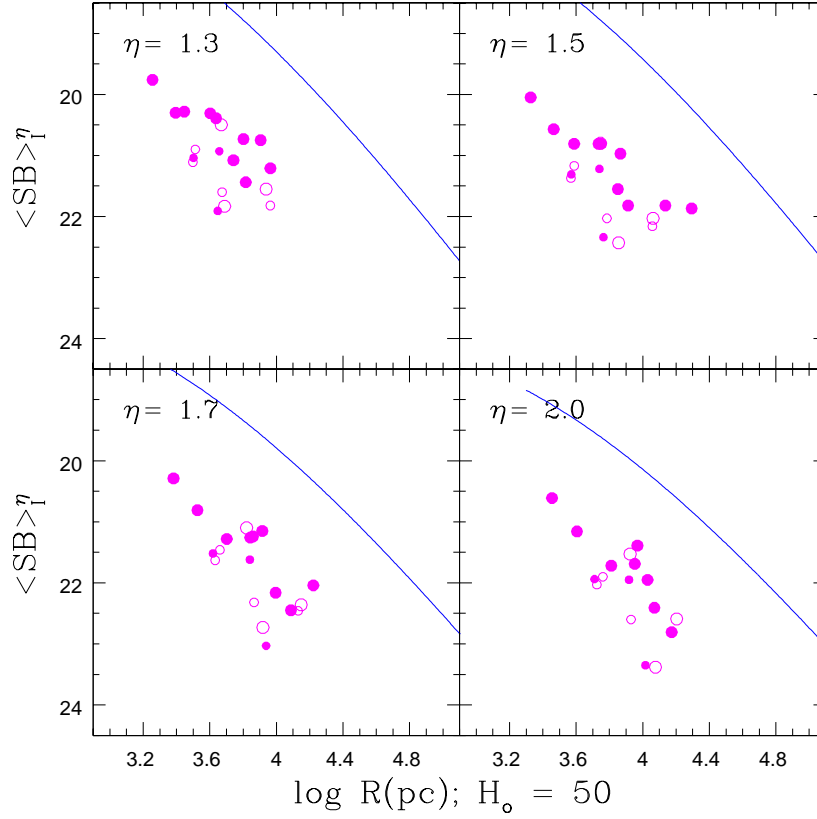


Fig. 2.— Same as Figure 1 but for the  $I$  band data for the two clusters Cl 1324+3011 at  $z = 0.7565$  (closed circles) and Cl 1604+4304 at  $z = 0.8967$  (open circles) from the data in Tables 3 and 4. The lines for zero redshift are the same as in Figure 1 but shifted to the  $I$  band by  $\langle R - I \rangle = 0.62$ .

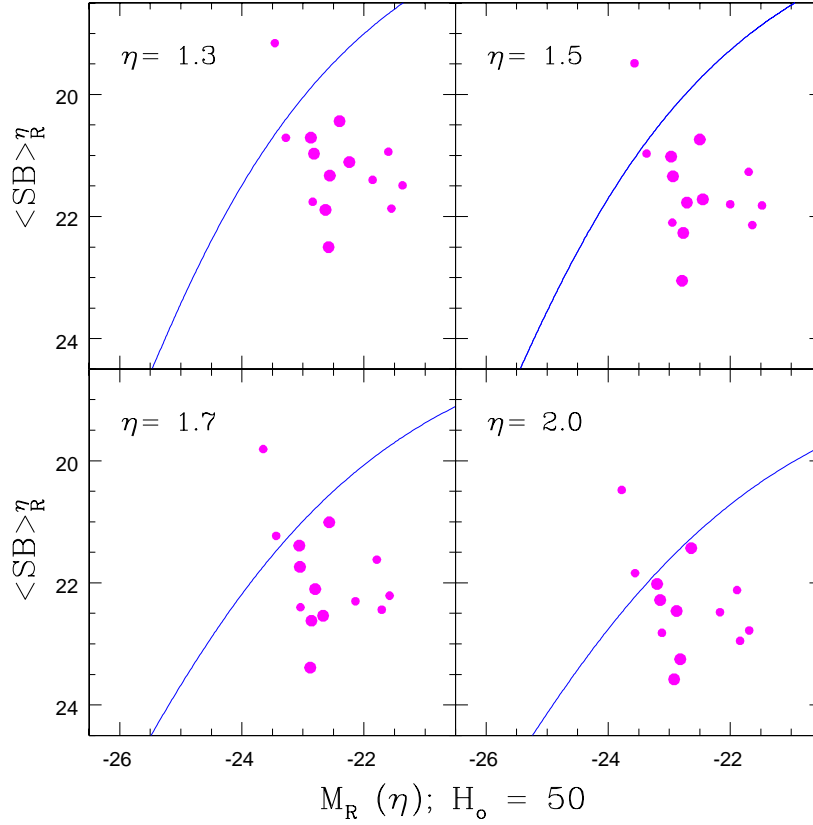


Fig. 3.— The  $M$ ,  $\langle SB \rangle$  diagram for Cl 1604+4321 from the data in Table 2 for the  $H_o = 50$ ,  $q_o = \frac{1}{2}$  model. The solid line is the zero-redshift calibration derived from the zero-redshift  $\log R$ ,  $\langle SB \rangle$  relation in Figure 1 and equation (11) of Paper I. The symbols are the same as in Figure 1.

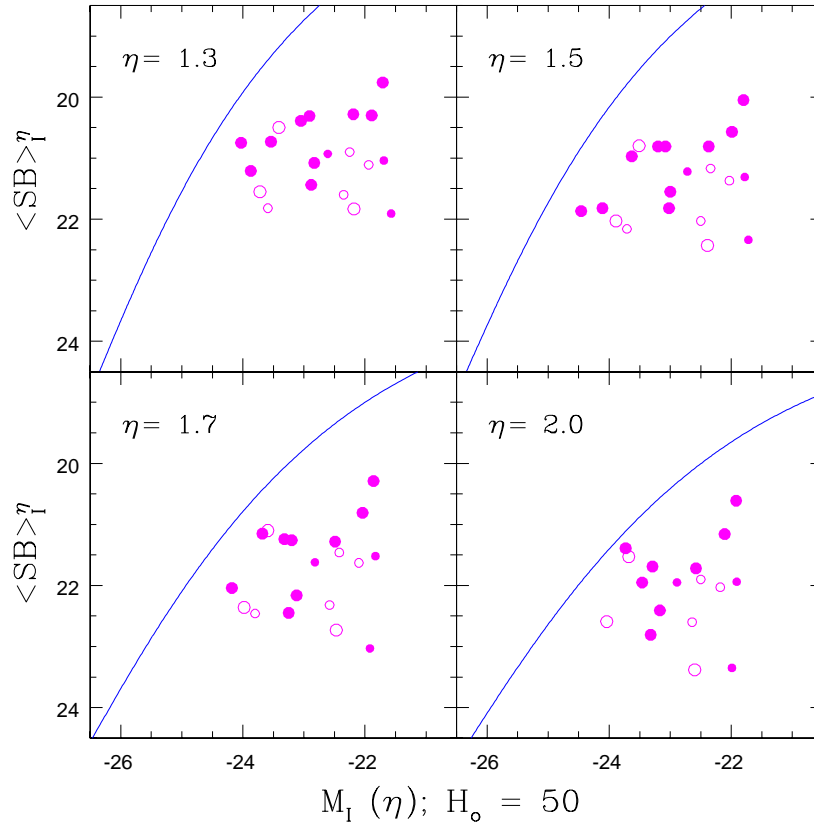


Fig. 4.— Same as Figure 3 for the  $M$ ,  $\langle SB \rangle_I$  diagram for the combined data for the clusters Cl 1324+3011 and Cl 1604+4304 from Tables 3 and 4. Closed and open circles are for Cl 1324+3011 and Cl 1604+4304, respectively.

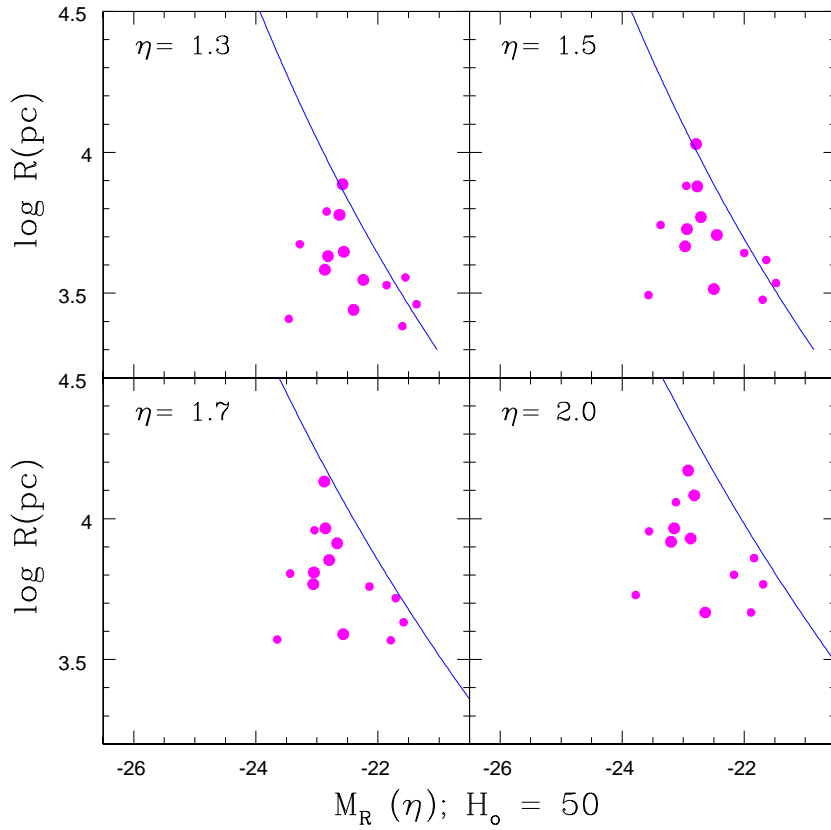


Fig. 5.— The deviation of the absolute magnitude at a given linear radius in the  $R$  photometric band from the zero-redshift correlation line for Cl 1604+4321. The solid line is the zero-redshift calibration derived from the zero-redshift  $\log R$ ,  $\langle SB \rangle$  relation in Figure 1 and equation (11) of Paper I. The increase in absolute luminosity that is required to preserve the  $(1+z)^4$  Tolman factor is the deviation toward brighter magnitudes seen relative to the zero-redshift line. This is clearly due to luminosity evolution. To preserve the Tolman factor requires that the evolutionary factor must be  $\langle \Delta M \rangle = 2.5 \log (1.9243)^{1.41} = 1.00$  mag for the weighted mean of the  $\eta$  values of 1.7 and 2.0. Because of the tautology of the argument, this diagram must show this factor, by necessity. The expectation from the theory of passive evolution is set out in §4.

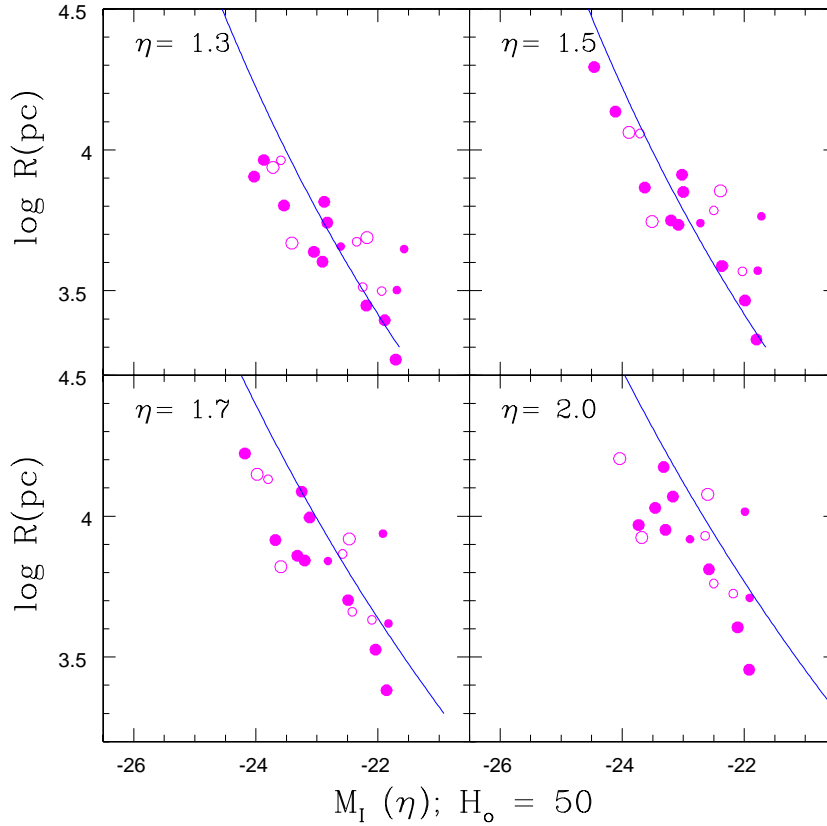


Fig. 6.— Same as Figure 5 but in the  $I$  photometric band for the two clusters Cl 1324+3011 ( $z = 0.7565$ ) and Cl 1604+4304 ( $z = 0.8967$ ). The tautological deviations in magnitudes from the zero redshift lines are required to be  $2.5 \log (1.7565)^{0.63} = 0.39$  mag and  $2.5 \log (1.8967)^{0.63} = 0.44$  mag, respectively, as the weighted mean of the  $\eta$  values of 1.7 and 2.0 if the expansion is real. These required evolutionary corrections are within the errors of the independent calculation of the evolution correction from the spectral synthesis calculations in §4 based on the observed colors.